UC Santa Barbara
UC Santa Barbara Previously Published Works

Title

A multi-tasking polypeptide from bloodworm jaws: Catalyst, template, and copolymer in film formation

Permalink

Journal

ISSN

Authors

Wonderly, William R
Nguyen, Tuan TD
Malollari, Katerina G
et al.

Publication Date

DOI

Copyright Information

Peer reviewed

Matter

Article

A multi-tasking polypeptide from bloodworm jaws: Catalyst, template, and copolymer in film formation
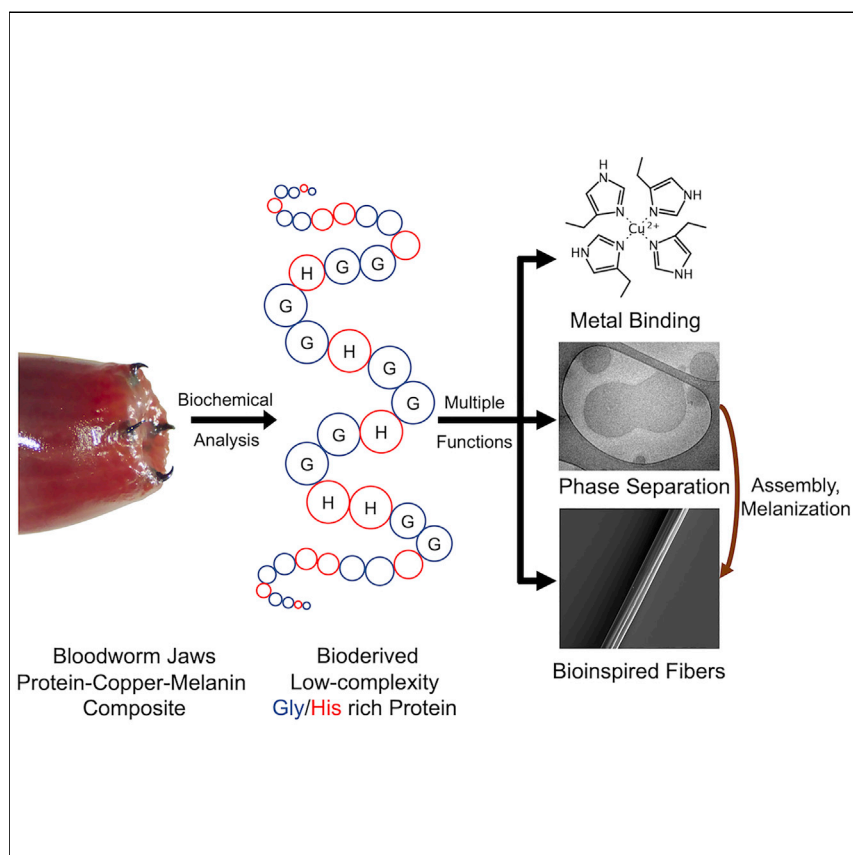
Melanin is a promising material but has significant challenges with synthesis and processing. Here, we study the melanized jaws of *Glycera dibranchiata* to understand how nature overcomes these challenges. We discover a protein with low sequence complexity that, through a variety of functions including metal binding and phase separation, facilitates the growth of thin melanized films.

William R. Wonderly, Tuan T.D. Nguyen, Katerina G. Malollari, ..., Phillip B. Messersmith, Matthew E. Helgeson, J. Herbert Waite

billywonderly@gmail.com (W.R.W.)
hwaite@ucsb.edu (J.H.W.)

Highlights

Identification of a low-complexity protein present in a crosslinked natural system

In vitro characterization of multipole protein functions

Metal-induced phase separation

Interfacial assembly, crosslinking, and thin film formation allows for fiber drawing

Demonstrate

4

Demonstrate
Proof-of-concept of performance with intended application/response

Article

A multi-tasking polypeptide from bloodworm jaws: Catalyst, template, and copolymer in film formation

William R. Wonderly,[1,*] Tuan T.D. Nguyen,[2] Katerina G. Malollari,[3] Daniel DeMartini,[4] Peyman Delparastan,[5] Eric Valois,[4] Phillip B. Messersmith,[5,6,7] Matthew E. Helgeson,[2] and J. Herbert Waite[1,4,8,*]

SUMMARY

Bloodworm jaws are composites of protein, melanin, and both mineral and ionic copper. To date, nanomechanical tests have correlated the ionic copper and melanin with hardness and wear resistance, but the function of protein is uncertain. Here, we characterize a Gly- and His-rich protein called multi-tasking protein (MTP) and, using recombinant protein, show that it performs six distinct functions critical for jaw formation and performance, namely (1) recruiting 22 equiv of Cu^{2+}, (2) mediating a liquid-liquid phase separation of the MTP-copper complex, (3) catalyzing the oxidation of 3,4-dihydroxyphenylalanine (Dopa) to melanin, (4) templating the interfacial polymerization of melanin, (5) integrating melanin and itself into thin films and fibers, and (6) providing intermolecular cohesion through Cu bridging. MTP achieves all these by assuming unprecedented roles as a building block, organizer, and fabricator—a processing feat of considerable relevance to the autonomous production of other polymer composites, blends, and/or networks.

INTRODUCTION

Synthetic hydrogels made from multiple polymer networks are renowned for their strength and toughness.[1,2] The same is true for anhydrous double polymer networks, although fabrication of these remains challenging.[3] As living organisms make both hydrogels and less hydrated varieties of tough polymer networks, a detailed study of formation strategies holds many potential insights. For example, vertebrate cartilage is a high-performance load-bearing hydrogel that is formed and maintained by isolated matrix-embedded cells known as chondrocytes that mediate simultaneous co-deposition and turnover of multiple polymer networks.[4] By contrast, in cell-free invertebrate cuticles, such as squid beak, a chitinous hydrogel is deposited first by epidermal cells and then infiltrated with liquid-liquid phase-separated proteins that displace water and harden following oxidation.[5] Here, we elucidate a third, previously unreported strategy in bloodworm jaws in which a suspension of metallo-protein droplets contributes catalytically and structurally to form a second melanin-like network *in situ*.

The bloodworm *Glycera dibranchiata* Ehlers, 1868, is a marine polychaete (phylum Annelida) that burrows through intertidal benthic mud to a depth of several meters. The proboscis of each worm is equipped with four black jaws (Figures 1A and 1B) that grasp and inject venom into other creatures during hunting and combat. The major

Progress and potential

High-performance natural materials play a critical role in informing modern material design and development. Bloodworm jaws, used for hunting and defense, are lightweight but with impressive impact and wear properties. The jaw composition is exotic at ~10% copper and a blend of equal parts of protein and melanin, a pigment rarely used in load-bearing functions. Much of jaw material production is dependent on the properties of the protein, which include binding copper, phase separation, catalyzing melanin formation, and assembling the protein-copper-melanin blend.

For effective technological translation, research needs to scrutinize the mechanisms of each of these properties and how they relate to one another. Copper binding underpins the formation of a dense protein liquid phase and enables melanin synthesis but later provides self-healing cohesive bridges between the proteins. The research has the potential to change the way we design, make, use, and dispose of our materials.
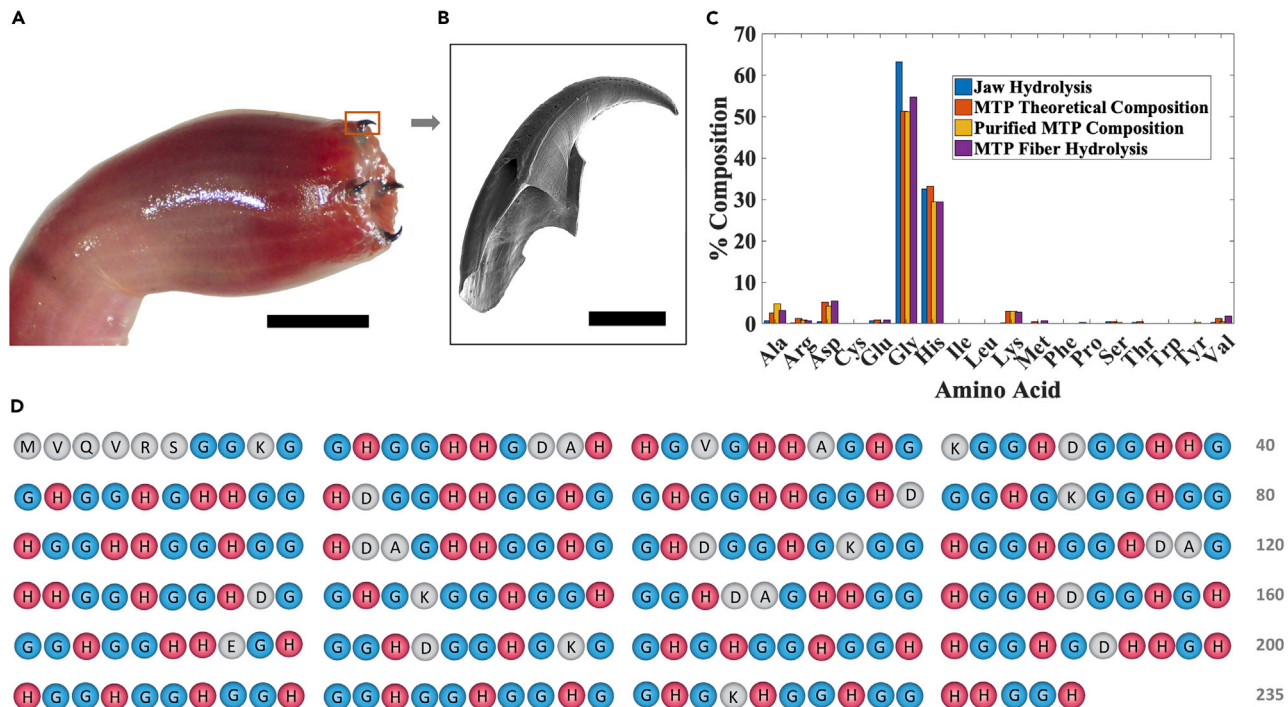
Figure 1. Structure and protein analysis of *Glycera* jaw

(A) Image of the everted proboscis of *Glycera dibranchiata* with its four jaws exposed.

(B) Scanning electron microscope image of a *Glycera* jaw. Scale bars, 0.5 mm.

(C) Amino acid composition of *Glycera* jaws (blue), theoretical amino acid composition of MTP (orange), experimental amino acid composition of purified MTP (yellow), and amino acid composition of the interfacial film formed when MTP is allowed to react with L-Dopa (purple).

(D) Sequence of MTP with glycine residues highlighted in blue and histidine residues in red for emphasis.

structural components of *Glycera* jaws are protein (~50% w/w), ionic and mineralized copper (up to 10%), and melanin (~40% w/w).[6,7] The presence of melanin is not unusual, as melanin is extensively used in biology as a pigment. Jaw melanin, however, is unique in existing as a contiguous material that is ~2 mm in length, thereby greatly exceeding the micrometer length scale typically associated with dispersions of melanin pigment, such as those found in *Sepia* ink or melanosomes.[8]

Melanin has many desirable properties,[9] but given that *in vitro* formation typically leads to dispersions of small (~100 nm diameter) granules,[8] applications of melanin in synthetic materials remain limited. The melanin and copper in *Glycera* jaws are correlated with impressive wear resistance,[10] and a deeper understanding of the mechanisms of their formation and function could lead to expanded use of melanin in high-performance materials. Although previous work has shown that the protein composition of whole jaws is dominated by glycine (Gly) (~50 mol %) and histidine (His) (~30 mol %),[6] the function of these Gly- and His-rich sequences is currently unknown.

Here, we identify and characterize properties of the primary structural protein in bloodworm jaws, hereafter named multi-tasking protein (MTP). *Glycera* MTP is a multi-functional molecule with the ability to chelate copper, phase-separate, induce the polymerization of L-3,4-dihydroxyphenylalanine (Dopa) to melanin, template the synthesis of macroscopic 2D melanin-protein composite films, and mediate their mechanical properties, all notwithstanding its sequence simplicity. The concerted activities of MTP in the construction of *Glycera* jaw architecture present a compelling

[1]Department of Chemistry & Biochemistry, University of California, Santa Barbara, Santa Barbara, CA 93106, USA

[2]Department of Chemical Engineering, University of California, Santa Barbara, Santa Barbara, CA 93106, USA

[3]Department of Mechanical Engineering, University of California, Berkeley, Berkeley, CA 94720, USA

[4]Department of Molecular, Cell, and Developmental Biology, University of California, Santa Barbara, Santa Barbara, CA 93106, USA

[5]Department of Materials Science and Engineering, University of California, Berkeley, Berkeley, CA 94720, USA

[6]Department of Bioengineering, University of California, Berkeley, Berkeley, CA 94720, USA

[7]Materials Sciences Division, Lawrence Berkeley National Laboratory, Berkeley, CA 94720, USA

[8]Lead contact

*Correspondence:
billywonderly@gmail.com (W.R.W.),
hwaite@ucsb.edu (J.H.W.)

opportunity to rethink the design of processing technologies needed for high-performance and sustainable composite and blended polymeric materials.

RESULTS

### *Glycera* jaws, transcriptomics, and protein sequence

The everted proboscis of a *G. dibranchiata* worm in Figure 1A highlights its four black jaws. The jaws are approximately 2 mm in length (Figures 1A and 1B) and have impressive mechanical properties that do not depend on mineralization.[10] *Glycera* jaws are highly sclerotized, with protein, copper ions/mineral, and melanin distributed throughout the hierarchical architecture.[6,7] The protein component has a composition dominated by two amino acids: Gly (>50 mol %) and His (>30 mol %) (Figure 1C). Undermined by the high degree of crosslinking in the jaw, protein extractions have consistently resulted in low yields, although sufficient amounts of a 30-kDa protein were obtained to prove that its amino acid composition matched that of the jaw.[11] From that point on, we have relied on state-of-the-art transcriptomic methods to investigate this peculiar protein.

Motivated by similar work on squid beak[5] and *Nereis* jaws,[12] the transcriptome generated from the jaw pulp of *G. dibranchiata* (the secretory epithelial tissue in contact with the base of the jaw and with histochemical properties similar to those of the jaw[13]) provided ~24,000 transcripts, the most highly represented being cytoskeletal proteins, such as actin and myosin. We identified assembled candidate sequences by searching the transcriptome for transcripts rich in both glycine and histidine. The most compelling candidate sequence is shown in Figure 1D and was chosen because it was a fully assembled transcript, containing a start codon, signal peptide, and stop codon. The predicted protein sequence composition also matched the amino acid composition of jaws (Figure 1C) and showed a similar composition and molecular weight of ~30 kDa (as determined by SDS-PAGE) to the protein purified from *G. dibranchiata* jaws in previous work.[11] We validated the sequence by traditional polymerase chain reaction (PCR) methods, cloning it from fresh cDNA generated from the jaw pulp with primers outside the coding sequence. The PCR product was sequenced by Sanger methods and successfully cloned expressed in *Escherichia coli*.

Consistent with an acid hydrolyzed jaw, the MTP sequence is dominated by Gly and His (over 80%). There are no instances of more than two Gly (G) or His (H) residues in a row, resulting in a sequence made up almost entirely of HGGH, GGH, or HGG repeats, depending on the point of reference. Typical BLAST searches of UniProtKB/Swiss-Prot databases returned no homologous sequences. Not surprisingly, the prevalence of Gly/His in MP does show similarities to that of another polychaete, *Nereis virens* jaw protein-1 (Nvjp-1),[12,14] although *Glycera* MTP lacks the abundant aromatic residues of Nvjp-1. The unusually high Gly content of MTP suggests flexibility and intrinsic disorder. High Gly content is found in a number of other structural proteins, such as plant cell wall glycine-rich proteins (60%–70%),[15] spider silk fibroin (47.3%),[16] collagen (~33%), and elastin (~30%).[17] Moreover, MTP adds to a growing number of Gly- and His-rich structural proteins found in invertebrates, including polychaete (*Glycera*/*Nereis*) jaws, squid beaks, *Hydra* nematocyst spines, insect mandibles, and spider fangs, and all are robust structures both with and without added metal ions.[18]

MTP structure and copper binding

The influence of pH and copper on MTP structure is shown in Figures S1 and S2. The CD spectrum at pH 5.0 exhibits an ellipticity minimum at 201 nm, and maxima at 195 and 220 nm. Upon increasing the pH to 7.4 the minimum is shifted to 195 nm, and
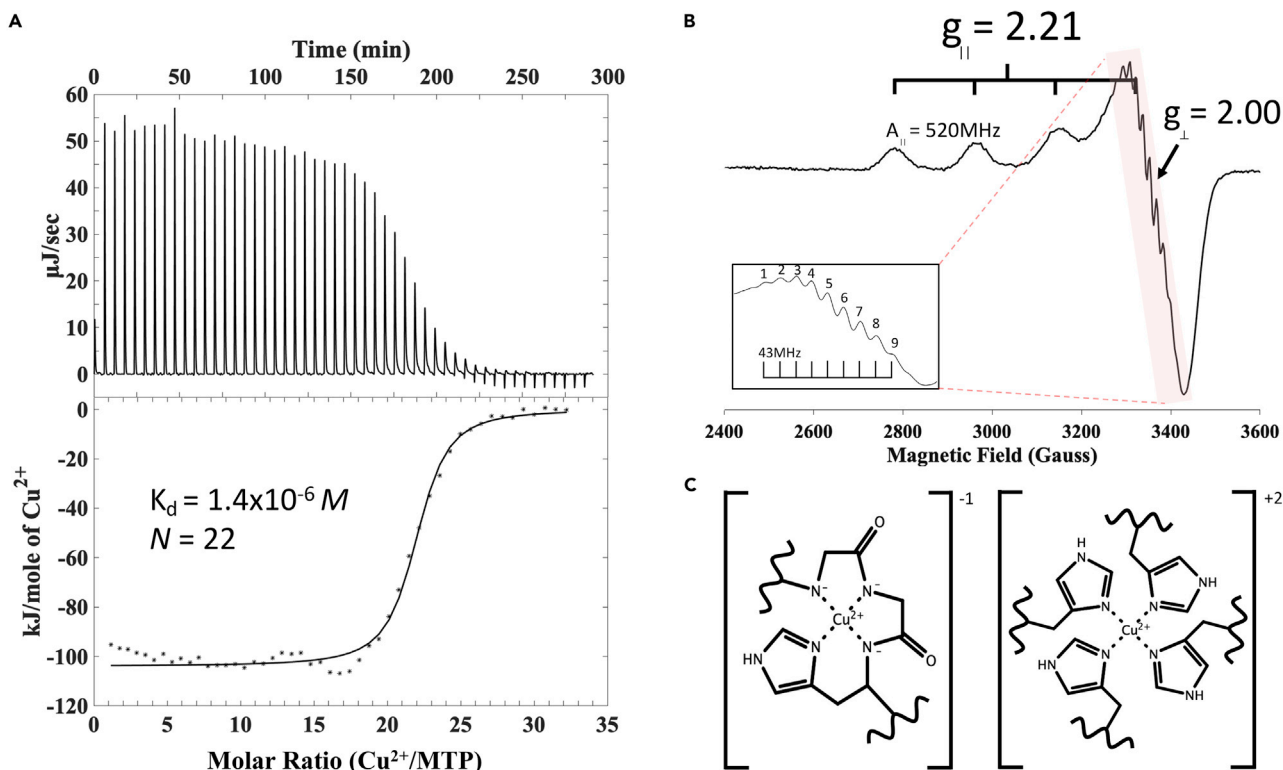
Figure 2. *In vitro* characterization of copper binding to MTP

(A) ITC thermogram for the titration of 3.3 mM CuSO$_4$ into 0.03 mM MTP at pH 7.4. The top panel shows the raw trace, and the bottom panel shows the integrated head profiles (*). The solid line is the nonlinear least squares fit to a model of multiple independent binding sites.

(B) X-band EPR spectrum of frozen 0.1 mM MTP in 100 mM Tris and 1 mM CuSO$_4$. The inset shows the nine-line super-hyperfine splitting present in the perpendicular region.

(C) Possible binding structures of copper to the protein either via backbone amides or through imidazole side chains.

the intensity of the maximum at 220 nm increases. The addition of copper at pH 7.4 does not result in an appreciable change in the CD spectrum. Although the CD spectrum does change with increasing pH, deconvolution of the spectra with the program BeStSel[19] estimates that all conditions represent a significant amount of random coil (>40%) and β sheet content (>40%). Hence the predicted flexibility is confirmed by CD measurements.

Copper binding ability of the MTP was investigated because the jaw contains significant quantities of copper (up to 10% by weight) that is both ionic and mineral. Isothermal titration calorimetry (ITC) confirmed that MTP has impressive copper binding capacity (Figure 2A). These data were fit to an independent model (NanoAnalyze software), which considers each binding site to be equivalent and independent and was chosen because of its simplicity and appropriateness in situations where the exact nature of the coordination is unknown.[20] We found an apparent equilibrium constant of K_{ITC} = 7.1 × 10^5 M and a binding capacity of N = 22 equiv of copper. A white precipitate was observed to form over time upon addition of excess copper ions.

ITC experiments thus support the notion that His contributes to copper binding. Under our experimental conditions, the apparent equilibrium constant of MTP with copper compares well with that of ceruloplasmin,[21] but is lower than that of other copper transport proteins, such as serum albumins. The more impressive aspect,

however, is the copper binding capacity (N = 22). When normalizing this value to protein MW we find MTP binds 1 Cu^{2+}/kDa, whereas ceruloplasmin binds 0.04 Cu^{2+}/kDa (assuming N = 9 Cu^{2+} and MW = 121 kDa) and binding stoichiometry for BSA is 0.08 Cu^{2+}/kDa (assuming N = 5 Cu^{2+} and MW = 66 kDa).[22]

Structure of the MTP-Cu complex

To investigate the structure of MP bound to copper, we performed low-temperature X-band continuous wave (CW) electron paramagnetic resonance (EPR) spectroscopy of MTP-Cu^{2+} complex in Tris buffer at pH 7.4. The spectrum reveals three clear low-field parallel lines with $g_\parallel$ = 2.21 and $A_\parallel$ = 520 MHz, with the fourth obscured by the perpendicular portion (Figure 2B). Simulation of the perpendicular region indicates a g value of 2.00. The low-field edge of the perpendicular region also shows at least nine well-resolved super-hyperfine lines separated by 43 MHz (Figure 2B, inset).

Although the copper binding properties are entirely predictable from the high histidine content, the coordination mode is not. The "GGH" motifs that make up the vast majority of the protein sequence are reminiscent of Gly/His model peptides that have been studied to mimic the amino terminal copper and nickel motif[23] as well as those synthesized to mimic the active site of Cu,Zn superoxide dismutase.[24–26] These peptides generally form square-planar complexes involving one or more Cu(II)-amide bonds. The nine-line super-hyperfine EPR splitting pattern and our EPR parameters of $g_\parallel$ = 2.21 and $A_\parallel$ = 520 MHz are consistent with coupling to four equatorial nitrogens.[27,28] However, it is unclear how many of these nitrogens are from the backbone or side-chain imidazole groups. Figure 2C posits copper complex geometries most consistent with these data.

Atomic force microscopy-assisted force spectroscopy

To provide more insight into the molecular phenomena underlying the metal-ligand interactions and high copper binding capacity of MTP, and to examine a potential mechanical role for these interactions, we performed single-molecule force spectroscopy (SMFS) experiments on MTP-Cu^{2+} films. SMFS is a powerful approach for investigating the molecular mechanics of macromolecules.[29–35] Here, we used SMFS to study the force-induced rupture of the inter- and intra-molecular His-Cu^{2+} interactions present in MTP-Cu^{2+} thin films. Figure 3A shows a schematic illustration of the simplest case of the SMFS experiments, in which atomic force microscopy (AFM) cantilevers were approached onto MTP-Cu^{2+} films deposited on TiO_2 substrates leading to nonspecific adsorption of a single, isolated protein to the cantilever, and then retracted while measuring the deflection of the cantilever. A characteristic feature of the retraction force-extension curves was the presence of multiple sequential dissociation events as indicated by a "sawtooth" pattern (Figure 3B) reminiscent of that observed upon unfolding of globular proteins under stretch.[30,34–38] The sawtooth features were not observed in control experiments performed on Cu^{2+}-free MTP films, leading us to conclude that each subpeak in the sawtooth pattern was the result of force-induced protein chain extension culminating in His-Cu^{2+} bond rupture, which in turn revealed previously unloaded chain segments (the so-called hidden length).[34–36] Although not reflected in Figure 3A, we note that the His-Cu^{2+} bonds may be either inter- or intra-molecular.

A worm-like chain (WLC) model was used to fit the rupture events to extract rupture force, contour length (L_c) values, and confirm single-molecule behavior. Figure 3C shows a histogram of rupture force distribution for His-Cu^{2+} interactions with an average of 268 ± 67 pN, stronger than typical hydrogen bonding (~100 pN) but weaker than covalent bonds (1–3 nN), in agreement with previous reports on the
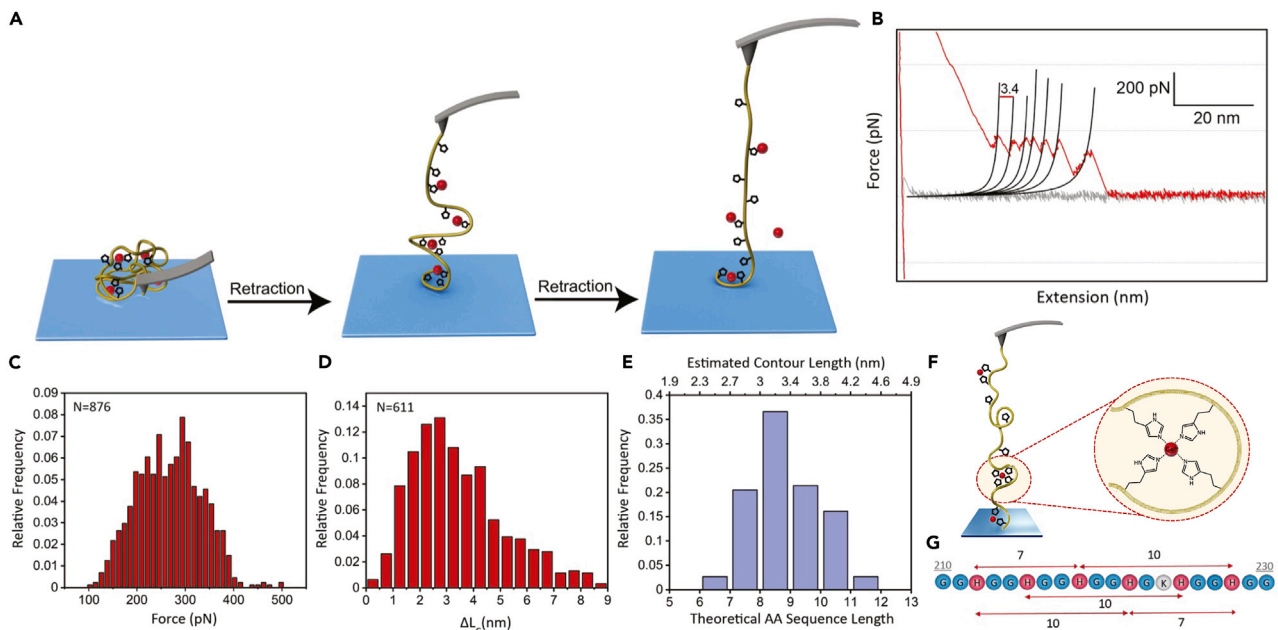
Figure 3. SMFS measurements on MTP-Cu²⁺ interactions

(A) Schematic illustration of the SMFS experiments assuming the simplest scenario in which a single chain is pulled in the absence of intermolecular complexes. Histidine side chains and copper ions are shown in black and red, respectively. Retraction of the cantilever results in sequential rupture of protein-Cu^{2+} interactions.

(B) A representative force-extension (F-X) curve is shown with approach and retraction traces in gray and red, respectively. The black lines correspond to the worm-like chain (WLC) fitting of the rupture events.

(C) Histogram of the rupture force distribution for MTP-Cu^{2+} interactions showing an average for 268 ± 67 pN.

(D) Histogram of incremental contour length increase distribution (ΔL_c) measured in SMFS experiments.

(E) Histogram of theoretical His-rich copper binding amino acid segment length based on the protein sequence considering formation of metal-ligand complexes involving three or four histidine side chains. Estimated contour length of the segments is calculated using a theoretical value of 0.38 nm for individual amino acid contour length.

(F) Force-induced MTP chain extension, leading to rupture of individual metal-ligand interactions, which in turn reveals the previously unloaded chain segments or the so-called hidden length (e.g., β turns in flexible MTP chains).

(G) Presence of His-rich motifs and example calculation of the theoretical amino acid segment length is shown for a selected region of MTP.

strength of metal-ligand and other non-covalent bonds.[34,35,39–41] It should be noted that a broad distribution of rupture forces is not unusual in SMFS due to the statistical nature of individual bond rupture; in this case, the broad distribution may partially reflect different pulling angles, heterogeneity in the attachment to the AFM probe, or multiple possible complexation environments in the MTP-Cu^{2+} complex, as a Cu^{2+} ion can be complexed by inter- or intra-molecular modes, or with one to four His and/or Gly residues.[35] Nonetheless, our SMFS results indicate the presence of relatively strong non-covalent interactions between Cu^{2+} and MTP, which would ultimately lend mechanical stability at the macroscopic level.[34,35,41]

Further analysis of the sawtooth pattern in force-extension curves revealed clear evidence for rupture events spaced at an average of 3.4 nm (Figure 3D). We defined the length increment between subsequent rupture events as ΔL_c, corresponding to the additional contour length released following sequential rupture events. Similar features have been previously reported for unfolding of repeat units in modular proteins or peeling of β strands from β sheets.[29,30,38,42] In the case of Cu^{2+} interacting with MTP, ΔL_c can be attributed to the release of previously unloaded β turns. Considering a theoretical length of 0.38 nm per amino
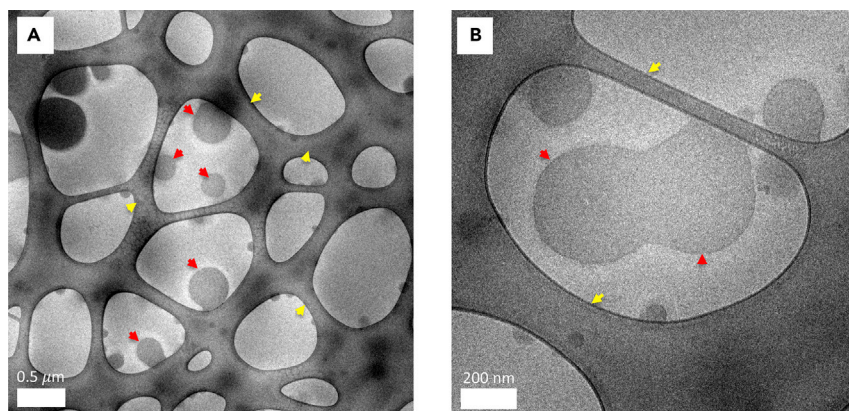
Figure 4. Copper-induced phase transition

(A) Cryo-TEM image of phase-separated droplets (red arrows) that form when 50 μM CuSO$_4$ is added to 5 μM MTP in 50 mM Tris buffer (pH 7.4) supported on a lacy carbon film (the contiguous phase indicated by yellow arrows).

(B) Cryo-TEM image showing the fusion of two droplets (red arrows) indicating their fluid behavior supported by lacy carbon (yellow arrows).

acid,[29,38,42,43] the ΔL_c obtained in our experiments corresponds to an average of ∼9 amino acid (aa) residues in the MTP sequence.

To better understand the possible underlying reasons for the measured ΔL_c distribution, we analyzed the MTP sequence to determine the length of possible His-rich Cu^{2+} binding motifs. Owing to the favorability of His-Cu^{2+} chelation thermodynamics and the high relative ratio of His to Cu^{2+} in our experiments (10 to 1), for our analysis we considered a segment of MTP containing three or four His residues as being capable of Cu^{2+} binding and calculated the lengths of all the possible segments that satisfy this condition (Figures 3E–3G). The theoretical distribution of lengths between binding sites is centered around ∼9 aa, consistent with the measured ΔL_c from SMFS experiments (Figures 3D and 3E). Interestingly, the average length of the Cu-binding sequence for MTP (∼9 aa) is close to the length of His-containing octarepeat domains (8 aa) in prion protein (PrP), a membrane-bound glycoprotein found in the nervous systems of different species.[44–46] PrP is comprised of an unstructured and flexible N-terminal region that contains fundamental eight-residue repeats essential for copper binding and neuroprotective self-regulation.[44,45]

Cu^{2+}-induced MTP liquid-liquid phase separation

The Cu^{2+}-dependent self-assembly of MTP was demonstrated by cryogenic transmission electron microscopy (cryo-TEM). In the presence of Cu^{2+} ions, MTP readily formed spherical droplets (Figures 4A and 4B, red arrows). These condensate droplets appeared to have no internal structure and were polydisperse, with diameters ranging from 50 nm to greater than 400 nm. The phase-separated material readily adsorbed to the lacy carbon support of the grids. Figure 4B shows two droplets fusing, indicating the fluid-like behavior of the condensed phase. Additional images of the phase-separated MTP are shown in Figure S3. We found no evidence of phase separation in the absence of copper (Figure S4).

MTP-Cu-assisted Dopa oxidation

The presence of melanin and copper in *Glycera* jaws, coupled with the high His content of MTP, prompted investigation of catechol oxidase (CO)-like activity because
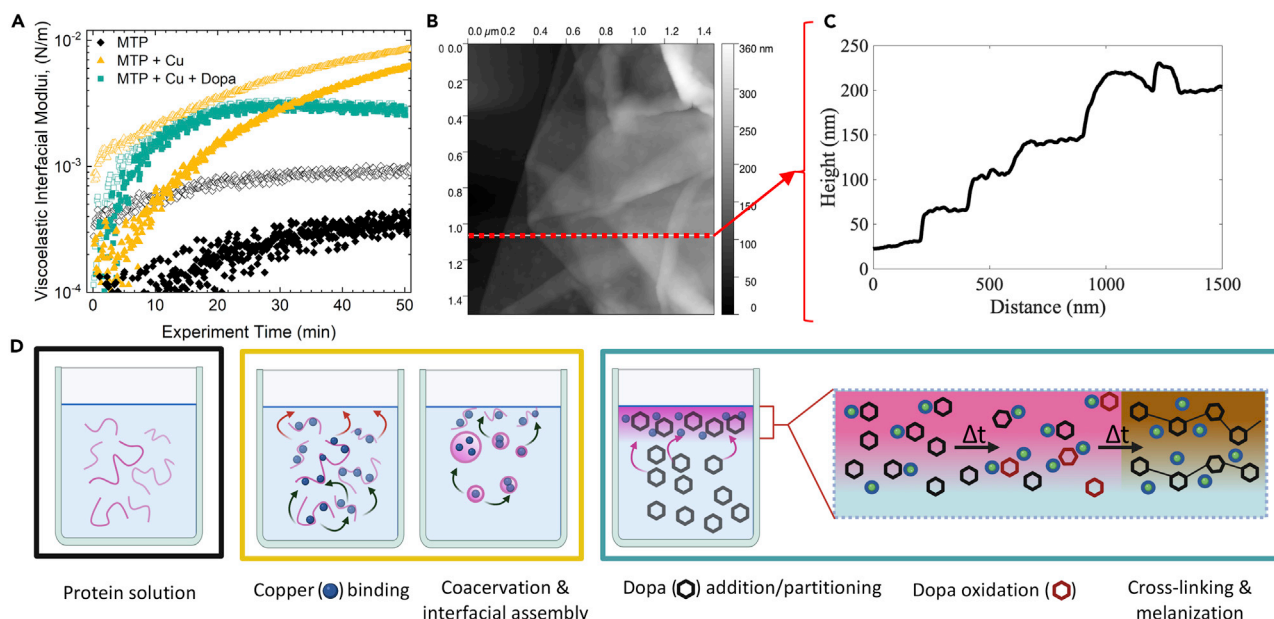
Figure 5. Interfacial activity of MTP

(A) Interfacial rheometry: The loss modulus (G'', open symbols) and storage modulus (G', filled symbols) as a function of time for 5 µM MTP solutions containing: no copper or dopa (black), 50 µM CuSO$_4$ (yellow), and 50 µM CuSO$_4$ and 500 µM L-Dopa (teal).

(B) AFM height trace of MTP catalyzed melanin film.

(C) The height profile of the red line in (B) shows that the sheets are 35–40 nm thick.

(D) A schematic model depicting the process causing the interfacial responses in (A). Copper binding induces proteins to surface assemble (red arrows), as well as coacervate and coalescence (green arrows). When present, Dopa molecules partition into the surface layer (grey arrows), where they undergo catalyzed oxidation, cross-linking, and melanization. Droplets have not coalesced significantly in the surface layer. The colored boxes around the cartoons are color-coordinated with the curves in (A).

the active CO site is characterized by a dinuclear copper center with each copper coordinated by three His residues.[47] An MBTH-coupled assay was used to determine the kinetic parameters of MTP engaging in catechol oxidation. When bound to 10 equiv of copper ions, and assuming that each bound copper is an independent active site, MTP was found to have a V_{max} = 0.9 ± 0.02 µM/min, K_m = 410 ± 8 µM (Figure S5), and k_{cat} = 0.18 ± 0.002 min^{-1}. Without copper present there was no detectable activity, suggesting that copper is necessary for the oxidizing capacity of MTP.

Despite our assuming ∼10 active sites, MTP displays a low reaction rate and an intermediate ability to bind L-Dopa.

Interfacial assembly and viscoelasticity

Interfacial shear rheometry was used to probe the assembly of MTP and the viscoelasticity of resulting films at an air-solution interface (Figure 5A). Buffered solutions containing 5 µM MTP were liquids (G'' ≫ G') with very low elastic (G') and viscous (G'') moduli. With the addition of 50 µM CuSO$_4$ (10 equiv), however, an interfacial film formed in ∼1 h. This film likewise showed liquid-like behavior throughout its maturation, but the values of G' and G'' increased steadily, indicating significant thickening of the interfacial film. When 0.5 mM L-Dopa was added to a solution mixture of 5 µM MTP and 50 µM CuSO$_4$, the interfacial film persisted; however, it showed signs of structural arrest (within 20 min) with a corresponding transition from a liquid to a viscoelastic film with G' ≈ G''.
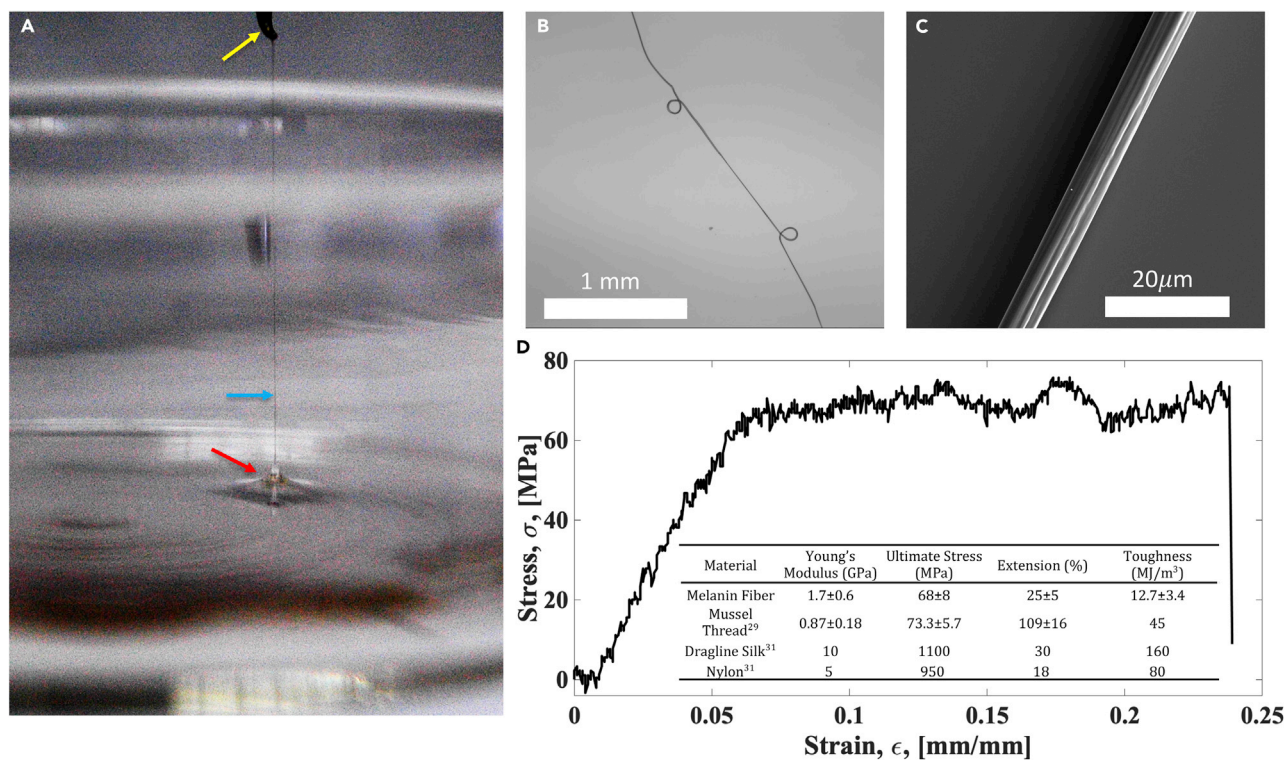
Figure 6. Interfacial film formation enables fiber drawing

(A) Image of the fiber-drawing process. A thick meniscus (red arrow) forms where the film begins to detach from the solution and collapse into a fiber (blue arrow) after being disturbed by a 1-mm diameter mechanical probe (yellow arrow).

(B) Optical microscope image of MTP-catalyzed fiber illustrating the length they can be pulled to. Scale bar, 1 mm.

(C) SEM image of a pulled fiber. Wrinkles are formed that align with the long axis of the fiber in the direction which they were pulled. Scale bar, 20 μm.

(D) Typical stress-strain curve of MTP-melanin fibers. Inset: table comparing the mechanical properties of MTP-melanin fibers and other biological fibers as well as nylon.

Material	Young's Modulus (GPa)	Ultimate Stress (MPa)	Extension (%)	Toughness (MJ/m^3)
Melanin Fiber	1.7±0.6	68±8	25±5	12.7±3.4
Mussel Thread[29]	0.87±0.18	73.3±5.7	109±16	45
Dragline Silk[31]	10	1100	30	160
Nylon[31]	5	950	18	80

MTP rapidly formed interfacial films when in the presence of both 10 equiv Cu (II) and 0.5 mM L-Dopa at pH 7.4. We monitored solution equilibrium by SDS-PAGE, which showed that the fluid was nearly MTP depleted within 1 h of Cu and Dopa addition (Figure S6). After ~30 min of reaction under these conditions, a transparent film formed at the air-water interface that, upon mechanical disruption, folded upon itself to form an insoluble black material. Alkaline peroxide (see supplemental information: materials and methods) was used to determine that sheets were 10% melanin by dry weight (Figure S7). Microscopic inspection of the precipitate (Figure S8) confirmed that the folded/bundled films appeared black and that individual films were transparent (Figure S8, red arrows). Analysis of films by scanning electron microscopy (SEM) detected large uniform sheets that, due to difficulty in sample manipulation, collapsed into pleated stacks (Figure S9). Films several square centimeters in area were readily made by spreading the reaction mixture out on glass Petri dishes. Further investigation by AFM showed that these sheets were 37 ± 2 nm thick (Figure 5C).

Fiber drawing and mechanics

Because films were confined to the air-water interface, we attempted to draw fibers from the MTP-melanin film in a manner not unlike the drawing of nylon from interfacial polymerizations.[48] A large meniscus formed upon contact with a metal probe and persisted during probe withdrawal from the surface of a freshly formed film

(Figure 6A). The interfacial film folded and compacted as it separated from the bulk and dried in air. Fibers several centimeters in length were readily drawn under these conditions. Typical fiber diameters were 7–11 μm as shown by SEM and light microscopy (Figures 6B and 6C). The SEM image shows fibers with wrinkles that align with the fiber long axis. Amino acid composition remained unchanged during film and fiber formation (Figure 1C, purple bars).

Fibers drawn from melanin-copper-protein films were pulled to failure as shown in Figure 6D. The fibers displayed an initial modulus of 1.7 ± 0.5 GPa, a yield strain of $6\% \pm 2\%$, and a maximum extensibility of $25\% \pm 5\%$ strain before failing. The average toughness of the fibers was 12.7 ± 3.4 MJ/m^3. The properties are summarized and compared with other biological and synthetic fibers (Figure 6D, inset table).[49–53]

DISCUSSION

Metal binding proteins are prominent adaptations, particularly in natural load-bearing systems,[18] and are becoming increasingly amenable to bio-inspired translation.[54] Using recombinant *Glycera* MTP, we have uncovered important principles of protein-mediated melanin synthesis *in vitro* that may inform our understanding of the jaw-building process. A key player in this process, MTP is remarkable for its simple sequence and multi-functionality.

The ~40 mol % His content of MTP enables a dramatic pH-triggered shift in the total protein charge, ranging from ~90% charged at one pH unit below the pK$_a$ of His (~6.5) and 90% uncharged at one pH unit above the pK$_a$. Given that proteins are stored at pH 5–6 before secretion, and that seawater pH is 8.2, the His-dependent pH trigger is a potent one.[31] This may also be related to the phase separation observed, which we hypothesize is due to coacervation. The copper-induced phase separation was somewhat unexpected as reversible metal-coordination-induced coacervation is a known phenomenon but somewhat rare.[55–57] We note, however, that intrinsically disordered[58] and low-complexity[59] proteins are often correlated with phase separation. That MTP-Cu apparently forms a condensed liquid phase is indicated by droplet coalescence (Figure 4B) and probably driven by a mechanism that depends on Cu-binding-dependent charging: the theoretic isoelectric point of MTP is ~7.4, and thus is neutral at the reaction pH. However, after binding to Cu^{2+} it will either gain a net positive charge if complexation is solely through imidazole groups, maintain neutrality if two amide nitrogen form coordinate bonds, or become net negatively charged if three amide nitrogen are recruited for the complexation (Figure 2C). Thus, the protein will have a combination of both uncharged and charged regions capable of facilitating separation of a dense protein-rich liquid phase. Based on the potential interfacial activity of the copper-bound protein, hydrophobic interactions exposed by His complexation with copper may contribute an additional driving force for phase separation. The droplet affinity for the lacy carbon support (Figures 4A and 4B) is consistent with the low interfacial tension of coacervate phase.[60]

The slow rate of catechol oxidation may be adaptive in the jaw system for kinetically controlled growth, as is often necessary for templating complex architectures.[61] Interfacial rheometry experiments were crucial for tracking reactivity and critical phase transitions in the maturation of MTP-derived films (Figure 5D). With no copper present, interfacial rheometry revealed a stable liquid behavior

in MTP. Upon addition of copper ions, the interfacial viscoelasticity increased steadily while maintaining liquid-like behavior (G''>G'). We propose that this is due to a combination of either charge-neutral coacervate droplets migrating to the hydrophobic air-water interface or the molecular adsorption of copper-bound protein complexes. The increased stiffness of films in the presence of Dopa provides further evidence of copper-bound MTP's ability to oxidize and react with Dopa.

Oxidation to quinones at the protein-rich interface (Figure 5D) created conditions ripe for melanin formation and/or reaction with the lysine or histidine residues of MTP, but further characterization would be required to confirm this.[62,63] The change in Dopa-dependent interfacial rheometry, the black color of the bundled sheets (Figure S8), and the alkaline peroxidation assay (Figure S7), confirm melanization of the films.

We have previously noted the unique choice of copper in the *Glycera* jaw system. What effect this choice has, especially when compared with other systems reinforced with metal ions, such as *Nereis* jaws or spider fangs, is complicated by the presence of both mineralized and ionic copper. A critical question at this time is to what extent the phase separation, oxidative capability, or metal binding capacity is unique to copper, or if other metal ions would yield similar results. A recent study showed that tau protein undergoes liquid-liquid phase separation triggered specifically by Zn^{2+}, which the authors attributed to low-affinity binding sites.[56] One possible mechanism that they suggest is that the coacervation of tau could be driven by transient intermolecular crosslinks formed with Zn^{2+} ions. A similar principle may be at play with MTP. Copper might form complexes with MTP that are sufficiently strong to promote association, but transient enough to lead to a coacervate rather than a solid precipitate. The use of a different metal ion would likely affect the oxidative behavior but would also strongly depend on the coordination chemistry, as is the case with copper.[64] Previous work showing the oxidative behavior of nickel bound to a Gly-Gly-His peptide suggests that this behavior may be retained.[65] If the oxidative behavior is unique to copper and if this capacity is maintained, it would lend some support to our previous hypothesis that, during injection, the venom undergoes catalytic conversion by the jaw surface.[6]

Depending on how Dopa partitions with regard to the droplets (Figures 7A and 7B), this either constrains the catalyzed oxidation of Dopa to dopaquinone at the droplet/aqueous phase interface, or within the droplets. Dopaquinone accumulation initiates formation of a second polymer (melanin). The coacervation and melanin partitioning displaces water, yielding an increasingly solid material and enabling tensile fibers to be drawn. The relatively high stiffness is likely due to the covalent and metal coordinate crosslinking of protein fibers by melanin. While melanin content of fibers (~10%) is lower than the roughly 40% melanin levels in native *Glycera* jaws, future work may find ways to increase film melanin content. Although the large extensibility is inconsistent with a covalently crosslinked system it is likely provided by the rupture of metal coordinate crosslinks, which both dissipates energy and reveals the hidden length of the protein components identified by our SMFS studies. The extension may also be provided by the gradual unwinding or tearing of bundled sheets. Satisfactory explanation of such properties awaits a better characterization of the relationship between MTP, melanin, and copper in the fibers.

These data may be suggestive of the early stages of jaw formation. We believe that it is unlikely that *Glycera* utilizes MTP exclusively to synthesize melanin *de novo* from
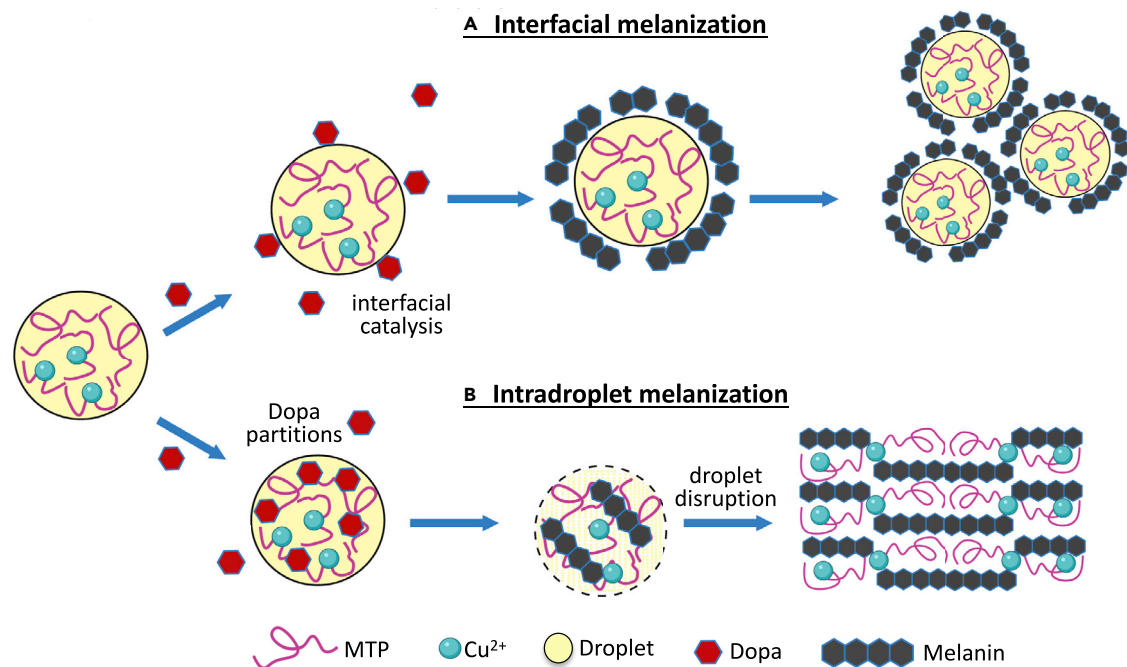
Figure 7. Two modes of MTP melanization depending on Dopa partitioning
(A) Dopa does not partition into droplets but is interfacially oxidized to melanin creating a coat.
(B) Dopa partitions into droplets where it gets oxidized and accumulates as melanin. Cu could contribute to crosslinking between melanin and MTP.

Dopa. More plausibly, MTP acts to oxidize the Dopa residues at the growing edge of the jaw thereby enabling crosslink formation between the protein and discrete melanin particles secreted by melanosomes during the formation of a contiguous scaffold. The protein's high degree of flexibility and multiple active sites helps facilitate this. We propose that the melanin eventually displaces water from the initial hydrogel and in the jaw. The combination of chemical simplicity and functional versatility in MTP holds tremendous potential for bio-inspired and natural materials processing.

EXPERIMENTAL PROCEDURES

Resource availability

Lead contact
Further information and requests for resources and reagents should be directed to and will be fulfilled by the lead contact, Herbert Waite (hwaite@ucsb.edu).

Materials availability
Protocols are provided for the synthesis and processing of the materials in this manuscript, and these materials are available upon reasonable request.

Data and code availability
Data used to support the conclusions in the paper are available from the corresponding author upon reasonable request.

Amino acid analysis
Samples for amino acid analysis were hydrolyzed with 6 M HCl, 1% phenol, *in vacuo* at 110°C overnight. HCl and phenol were removed under vacuum with a Savant SpeedVac SC110. After washing the residues with water and methanol, the samples

were reconstituted in 0.2 N HCl. Amino acid compositions were determined on a Hitachi L8900 amino acid analyzer system.

Transcriptome generation and assembly

Live *G. dibranchiata* specimens were purchased from the Bloodworm Depot (Whitefield, ME) and the jaws were dissected immediately. The connective tissue and musculature on the outside of the jaw was carefully removed under a dissecting microscope. Tissue inside the base of the jaw, however, was undisturbed. Samples were stored in RNA*later* (Invitrogen, Carlsbad, CA) and flash frozen in liquid nitrogen. Homogenization of the samples was performed under liquid nitrogen with a mortar and pestle, after which RNA was purified using a PureLink RNA Isolation Kit (Thermo Fisher Scientific, Waltham, MA) following the manufacturer's instructions. Four jaws from the same worm were used for RNA isolation. Total RNA samples were sent to myGenomics (Atlanta, GA) and paired-end sequenced (2 × 150 bp) on an Illumina HiSeq 2500 platform (Illumina, San Diego, CA). The raw sequencing data were analyzed using the Galaxy bioinformatics program.[66] We used the read processing tool Trimmomatic to remove adapter sequences and low-quality reads. The trimmed reads were then assembled into mRNA isotigs using the Trinity software package.[67] To estimate the transcription level of each isotig we used the software RSEM[68] to correlate trimmed reads with assembled transcripts. To identify candidates for the jaw proteins of *Glycera* we searched for sequences based on three criteria: (1) the presence of a signal peptide, (2) the presence of a stop codon, and (3) glycine and histidine contents of greater than 30% and 20%, respectively.

PCR validation and molecular cloning

We verified the presence of the *Glycera* jaw protein using PCR (GenBank: ON226769). A cDNA library was prepared with a SuperScript III RT-PCT (Invitrogen) kit following the manufacturer's instructions. The primers used were: (5′) CAT ATG GTG CAA GTA AGA AGT GGC and (3′) AAG CTT GTG TCT TCG GTG TAG GTG ACA TCC (note: *Hind*III and *Nde*I restriction sites were added for further subcloning). The PCR products were cloned into pCR4 vectors using a TOPO-TA Cloning Kit (Invitrogen), transformed into chemically competent TOP10 *E. coli* (Invitrogen), and grown on Luria-Bertani (LB) agar plates with kanamycin. Positive clones were grown over night in LB medium and the plasmid DNA was purified using a GeneJET Plasmid Miniprep Kit (Thermo Fisher) following the manufacturer's instructions. The plasmids were sequenced by Sanger sequencing (Genewiz, Newbury Park, CA). The constructs were subcloned into the pET-26b(+) vector (Novagen) and transformed into TOP10 cells for maintenance.

Recombinant expression and purification

We expressed the protein by freshly transforming the pET-26b(+) construct in BL21-(DE3)pLysS (Promega, Madison, WI) cells according to the manufacturer's instructions. Cells were screened by growth on LB agar with kanamycin and chloramphenicol, and colonies were maintained at 4°C. Selected colonies were grown overnight in 10 mL of LB medium augmented with 0.1% glucose (to further reduce basal expression), kanamycin, and chloramphenicol at 37°C. Saturated cultures were transferred into 1 L of Terrific Broth supplemented with 0.1% glucose, and grown at 30°C to an optical density of ∼0.6 at 600 nm. Expression was induced by the addition of isopropyl 1-thio-β-D-galactopyranoside to a final concentration of 1 mM. Cells were expressed for ∼12 h, after which they were pelleted by centrifugation (10 min, 5,000 × *g*), washed with buffer (20 mM Tris, 100 mM NaCl, 0.1 mM EDTA [pH 7.4]) and pelleted by centrifugation (10 min, 5,000 × *g*). Cell pellets were stored at −80°C until use.

Bacteria were resuspended in lysis buffer (20 mM Tris, 100 mM NaCl, 7 M urea [pH 7.4]) with 100 mM imidazole, and lysed via sonication on ice (5 × 30 s, 7 mW). The cell lysate was centrifuged at 10,000 × g. The supernatant was applied to a HisTrap FF immobilized metal affinity column charged with Ni(SO$_4$) and equilibrated with lysis buffer. Unbound protein was removed by successive washes of lysis buffer with 100 and 300 mM imidazole. Bound protein was eluted by washing with 500 mM imidazole in lysis buffer. Fractions with pure protein were identified by SDS-PAGE, acidified by the addition of 0.1% trifluoroacetic acid, and desalted using reversed-phase C8 HPLC. Protein was concentrated with lyophilization, after which it was reconstituted in Milli-Q water and kept at −80°C. We performed quantitative amino acid analysis to confirm the protein identity as well as estimate protein concentration.

ITC

A Nano ITC (TA Instruments, New Castle, DE) was used to measure the thermodynamics of copper binding to the *Glycera* jaw protein. In general, the sample cell was filled with in 950 μL of 10 μM *Glycera* jaw protein freshly dissolved in of sample buffer (10 mM Tris [pH 7.4]) at a final concentration of 10 μM. A solution of 3 mM CuSO$_4$ in 10 mM Tris (pH 7.4) was loaded into the syringe. Titrations were carried out as a sequence of 40 injections of 4.86 μL, with the stirring speed set at 250 rpm and the temperature set to 20°C. Control titrations were carried out to account for buffer mismatch (titrating copper solution into buffer only) and heat of dilution (titrating buffer into the protein solution). The final data were fit using the independent model provided in the NanoAnalyze software (version 3.3) and an independent model.

CW EPR

EPR was performed on a freshly prepared samples of 5 μM MTP and 50 μM CuSO$_4$ in 50 mM Tris buffer (pH 7.4). A volume of 0.5 mL was added to a 4-mm inner diameter quartz EPR tube (Wilmad). A Bruker EMXplus EPR spectrometer operating at 9.6 GHz and equipped with a Bruker ER 4119HS-LC High Sensitivity Probehead was used to collect the X-band EPR spectrum. Spectra were acquired at 140 K using 2.0 mW microwave power, 6.0 G modulation amplitude, 3,000 G sweep width, and averaging 32 scans.

Cryo-TEM

Samples of 5 μM MTP with and without 50 μM CuSO$_4$ were prepared in 100 mM Tris buffer (pH 7.4). Typically, a 2-μL of sample was pipetted onto a copper grid coated with lacey carbon, blotted with filter paper (Vitrobot Mark IV, FEI), and then quickly submerged in liquid ethane. Samples were loaded with a Gatan Cryo Transfer Holder maintained at −180°C. Imaging was performed with an FEI Tecnai G2 20 microscope operated at 200 kV.

CO activity assay

A 3-methyl-2-benzothiazolinone hydrazone hydrochloride (MBTH)-based assay was used to measure CO activity.[69] The buffer for the reaction contained 100 mM Tris, 4% DMF (v/v), and 6 mM MBTH. MTP was used at a final concentration of 5 μM and, when indicated, CuSO$_4$ was added to a final concentration of 50 μL. L-Dopa was the substrate and added at concentrations of 0.01, 0.1, 0.2, 0.5, 1, and 2 mM. The final reaction volume was 250 μL. Reactions were carried out at room temperature using a 96-well plate (Greiner) and each done in triplicate. The reaction was monitored at 505 nm every minute with a SpectraMax microplate reader (Molecular Devices). We used the molar extinction coefficient of the Dopachrome-MBTH adduct (28,900 M^{-1} cm^{-1})[70] to report reaction rates as change in concentration with time. The data were fit to the Michaelis-Menten model.

Film growth and fiber drawing

Films were grown by preparing a 1-mL solution with 4.5 μM protein (0.1 mg/mL), 45 μM $CuSO_4$, and 500 μM L-Dopa in 100 mM Tris buffer (pH 7.4). Sheet formation was not observed at pH 6 or below. We spread the solution on a clean microscope slide and, generally after ~30 min, the film had formed, identified under a dissecting microscope after agitation of the surface with a clean syringe needle. Samples for SEM and AFM were prepared by dipping a clean silicon coupon on the top of a solution with a freshly prepared film after 30 min of reaction. These samples were allowed to dry, washed extensively with water, and dried again under vacuum.

Fibers were prepared from freshly prepared films as described for sheet preparation. After 30 min of formation, fibers were drawn by touching a clean metal dissecting probe into the freshly formed film and pulling the probe slowly away from the solution. A slow rate is necessary to maintain fiber integrity. Fibers were stored in a desiccating chamber until tensile testing. Fibers kept in a humidity chamber would partially splay out and regain some sheet character.

Alkaline peroxide degradation to quantify melanin

A spectrophotometric assay of the solubilization of melanin by an alkaline peroxide solution was used to quantify the melanin content of the interfacial product. In the presence of H_2O_2 at alkaline pH and at high temperature, melanin will degrade into pyrrole-based chromophores.[71–73] The absorption of these products at 560 nm has a linear relation to the amount of melanin degraded.[7] Aqueous suspensions of synthetic melanin at concentrations of 0.1, 0.25, 0.5, 0.75, and 1 mg/mL were used to generate a standard curve. Melanin was dissolved by the addition of one part 10 N NaOH and two parts 30% H_2O_2 to 37 parts sample suspended in water followed by incubation at 70°C for 30 min. The interfacial films were dissolved in an identical manner to afford a solution at a concentration of 4 mg/mL. The absorbance of each sample at 560 nm was then measured. The best fit line for the melanin standard was forced through zero and gave an R^2 = 0.9983.

SEM

Interfacial sheets were polymerized as described above. The interfacial sheet was transferred to a small silicon coupon by bringing the coupon in contact with the surface of the reaction for 10 s. After drying under vacuum, the sample was gently washed three times with 1 mL of Milli-Q water. After attachment to an imaging stub, the sample was sputter-coated with a thin layer of gold for 100 s using an Anatech USA Hummer 6.2 coater. A FEI Nano Nova 640 FEG SEM was used to observe the samples.

Interfacial rheometry

Interfacial rheology was measured using a double-walled ring metal geometry attached to a stress-controlled rheometer (AR-G2, TA Instruments). Samples were loaded into a stepped annular trough made from Delrin, with radii as specified previously[74] and a trough depth of 2 mm. To probe the evolution of interfacial viscoelasticity, storage (G′) and loss (G″) moduli were recorded in response to an inputted small amplitude oscillatory strain with amplitude of 1% and a frequency of 2 Hz. Based on geometric and material parameters, the Boussinesq number was at least $O(10^2)$, which indicates that measurements were appropriately probing interface-dominated behavior.

To minimize time between loading the sample and starting the measurement, the location of the liquid-air interface was first determined for a trough filled with water

by carefully adjusting the geometry height until full capillary contact was observed. For samples loaded afterward, the geometry was immediately moved to the known position of the interface.

AFM imaging
Samples of interfacial films were allowed to form on glass microscope slides for 30 min. The films were transferred by contacting a mica sheet with the surface for several seconds to allow the films to adsorb. The films were then allowed to dry and washed with Milli-Q water. These samples were then imaged using an MFP-3D Bio AFM (Asylum Research, Goleta, CA).

AFM-assisted force spectroscopy
SMFS experiments were performed using a JPK ForceRobot 300 AFM (JPK Instruments, Berlin, Germany). Soft silicon nitride cantilevers (MLCT from Bruker Nano, USA) with a typical spring constant of 50–60 pN/nm were used. SMFS samples were prepared by drop casting an aqueous mixture solution of MTP and Cu^{2+} (as $CuSO_4$) at final concentrations of 4.5 and 36 μM, respectively, in 100 mM MOPS buffer (pH 7.4) on TiO_2 substrates. The $MTP-Cu^{2+}$ film casted TiO_2 substrates were briefly rinsed with 1 mL buffer and placed in an AFM sample holder, which was later filled with 100 mM MOPS buffer (pH 7.4). Data obtained in the SMFS experiments were analyzed using the JPK data processing software and a home-written procedure in IgorPro (Wavemetrics) for fitting the stretching events in the F-X curves with the WLC model to measure the corresponding rupture force and contour length. Histograms of the rupture forces and contour lengths were plotted using the OriginPro software. More detailed information is provided in the supplemental information.

Tensile testing
The ends of dry fibers were clamped with stainless steel grips. We estimated cross-sectional area by analyzing diameters of microscope images of each fiber and assuming a cylindrical geometry. The samples were loaded securely between grips and tested using a Nanobionix tensile tester (MTS). The samples were tested at ambient humidity and temperature. Stress-strain curves were taken at a strain rate of 0.1 min^{-1} and each sample was loaded to failure.

AUTHOR CONTRIBUTIONS
W.R.W. and J.H.W. initiated and planned the project. W.R.W. performed the sample preparation, recombinant expression and purification, ITC, CD, EPR, biochemical analyses, and tensile testing. T.N. performed the interfacial rheometry. D.D. performed the transcriptomic analysis. E.V. performed the AFM measurement. K.M. performed the SMFS. K.G.M., P.D., and P.B.M. analyzed the SMFS data. W.R.W. and J.H.W. wrote the manuscript. M.E.H. made edits and revisions on the final draft.

DECLARATION OF INTERESTS

The authors declare no competing interests.

REFERENCES

1. Dragan, E.S. (2014). Design and applications of interpenetrating polymer network hydrogels. A. Review. Chem. Eng. J. *243*, 572–590. https://doi.org/10.1016/j.cej.2014.01.065.

2. Fan, H., and Gong, J.P. (2020). Fabrication of bioinspired hydrogels: challenges and opportunities. Macromolecules *53*, 2769–2782. https://doi.org/10.1021/acs.macromol.0c00238.

3. Ducrot, E., Chen, Y., Bulters, M., Sijbesma, R.P., and Creton, C. (2014). Toughening elastomers with sacrificial bonds and watching them break. Science *344*, 186–189. https://doi.org/10.1126/science.1248494.

4. Halloran, J.P., Sibole, S., van Donkelaar, C.C., van Turnhout, M.C., Oomens, C.W.J., Weiss, J.A., Guilak, F., and Erdemir, A. (2012). Multiscale mechanics of articular cartilage: potentials and challenges of coupling musculoskeletal, joint, and microscale computational models. Ann. Biomed. Eng. *40*, 2456–2474. https://doi.org/10.1007/s10439-012-0598-0.

5. Tan, Y., Hoon, S., Guerette, P.A., Wei, W., Ghadban, A., Hao, C., Miserez, A., and Waite, J.H. (2015). Infiltration of chitin by protein coacervates defines the squid beak mechanical gradient. Nat. Chem. Biol. *11*, 488–495. https://doi.org/10.1038/nchembio.1833.

6. Lichtenegger, H.C., Schöberl, T., Bartl, M.H., Waite, H., and Stucky, G.D. (2002). High abrasion resistance with sparse mineralization: copper biomineral in worm jaws. Science *298*, 389–392. https://doi.org/10.1126/science.1075433.

7. Moses, D.N., Harreld, J.H., Stucky, G.D., and Waite, J.H. (2006). Melanin and Glycera jaws. J. Biol. Chem. *281*, 34826–34832. https://doi.org/10.1074/jbc.M603429200.

8. Clancy, C.M.R., and Simon, J.D. (2001). Ultrastructural organization of eumelanin from Sepia officinalis measured by atomic force microscopy. Biochemistry *40*, 13353–13360. https://doi.org/10.1021/bi010786t.

9. Hill, H.Z. (1992). The function of melanin or six blind people examine an elephant. BioEssays *14*, 49–56. https://doi.org/10.1002/bies.950140111.

10. Pontin, M.G., Moses, D.N., Waite, J.H., and Zok, F.W. (2007). A nonmineralized approach to abrasion-resistant biomaterials. Proc. Natl. Acad. Sci. *104*, 13559–13564. https://doi.org/10.1073/pnas.0702034104.

11. Moses, Dana Novak (2007). Structure, Biochemistry, and Mechanical Properties of Glycera Marine Worm Jaws, (ProQuest Dissertations & Theses A&I) UMI (University of California), p. 3285839.

12. Broomell, C.C., Chase, S.F., Laue, T., and Waite, J.H. (2008). Cutting edge structural protein from the jaws of Nereis virens. Biomacromolecules *9*, 1669–1677. https://doi.org/10.1021/bm800200a.

13. Michel, C., Fonze-Vignaux, M.T., and Voss-Foucart, M.F. (1973). Données nouvelles sur la morphologie, l'histochimie et la composition chimique des machoires de Glycera convoluta Keferstein (Annélide Polychète). Bull. Biol. Fr. Belg. *107*, 301–321.

14. Voss-Foucart, M.-F., Fonze-Vignaux, M.-T., and Jeuniaux, C. (1973). Systematic characters of some polychaetes (Annelida) at the level of the chemical composition of the jaws. Biochem. Syst. Ecol. *1*, 119–122. https://doi.org/10.1016/0305-1978(73)90025-2.

15. Ringli, C., Keller, B., and Ryser, U. (2001). Glycine-rich proteins as structural components of plant cell walls. Cell. Mol. Life Sci. *58*, 1430–1441. https://doi.org/10.1007/PL00000786.

16. Xu, M., and Lewis, R.V. (1990). Structure of a protein superfiber: spider dragline silk. Proc. Natl. Acad. Sci. U S A. *87*, 7120–7124. https://doi.org/10.1073/pnas.87.18.7120.

17. Brown-Augsburger, P., Tisdale, C., Broekelmann, T., Sloan, C., and Mecham, R.P. (1995). Identification of an elastin cross-linking domain that joins three peptide chains. J. Biol. Chem. *270*, 17778–17783. https://doi.org/10.1074/jbc.270.30.17778.

18. Degtyar, E., Harrington, M.J., Politi, Y., and Fratzl, P. (2014). The mechanical role of metal ions in biogenic protein-based materials. Angew. Chem. Int. Ed. *53*, 12026–12044. https://doi.org/10.1002/anie.201404272.

19. Micsonai, A., Wien, F., Kernya, L., Lee, Y.-H., Goto, Y., Réfrégiers, M., and Kardos, J. (2015). Accurate secondary structure prediction and fold recognition for circular dichroism spectroscopy. Proc. Natl. Acad. Sci. *112*, E3095–E3103. https://doi.org/10.1073/pnas.1500851112.

20. Srivastava, V.K., and Yadav, R. (2019). Isothermal titration calorimetry. In Data Processing Handbook for Complex Biological Data Sources (Elsevier), pp. 125–137. https://doi.org/10.1016/B978-0-12-816548-5.00009-5.

21. Zgirski, A., and Frieden, E. (1990). Binding of Cu(II) to non-prosthetic sites in ceruloplasmin and bovine serum albumin. J. Inorg. Biochem. *39*, 137–148. https://doi.org/10.1016/0162-0134(90)80022-P.

22. Masuoka, J., Hegenauer, J., Van Dyke, B.R., and Saltman, P. (1993). Intrinsic stoichiometric equilibrium constants for the binding of zinc(II) and copper(II) to the high affinity site of serum albumin. J. Biol. Chem. *268*, 21533–21537. https://doi.org/10.1016/S0021-9258(20)80574-2.

23. Harford, C., and Sarkar, B. (1997). Amino terminal Cu(II)- and Ni(II)-Binding (ATCUN) motif of proteins and peptides: metal binding, DNA cleavage, and other properties. Acc. Chem. Res. *30*, 123–130. https://doi.org/10.1021/ar9501535.

24. Casolaro, M., Chelli, M., Ginanneschi, M., Laschi, F., Messori, L., Muniz-Miranda, M., Papini, A.M., Kowalik-Jankowska, T., and Kozłowski, H. (2002). Spectroscopic and potentiometric study of the SOD mimic system copper(II)/acetyl-l-histidylglycyl-l-histidylglycine. J. Inorg. Biochem. *89*, 181–190. https://doi.org/10.1016/S0162-0134(02)00365-3.

25. Jancsó, A., Paksi, Z., Jakab, N., Gyurcsik, B., Rockenbauer, A., and Gajda, T. (2005). Solution chemical properties and catecholase-like activity of the copper(ii)–Ac-His-His-Gly-His-OH system, a relevant functional model for copper containing oxidases. Dalt. Trans. 3187–3194. https://doi.org/10.1039/b507655b.

26. Bonomo, R.P., Impellizzeri, G., Pappalardo, G., Purrello, R., Rizzarelli, E., and Tabbì, G. (1998). Co-ordinating properties of cyclopeptides. Thermodynamic and spectroscopic study on the formation of copper(II) complexes with cyclo(Gly-His)4 and cyclo(Gly-His-Gly)2 and their superoxide dismutase-like activity. J. Chem. Soc. Dalt. Trans. 3851–3858. https://doi.org/10.1039/a804481c.

27. Szabó-Plánka, T., Peintler, G., Rockenbauer, A., Győr, M., Varga-Fábián, M., Institórisz, L., and Balázspiri, L. (1989). Electron spin resonance study of copper(II) complexes of X-glycine and glycyl-X type dipeptides, and related tripeptides. Variation of co-ordination modes with ligand excess and pH in fluid and frozen aqueous solutions. J. Chem. Soc. Dalt. Trans. 1925–1932. https://doi.org/10.1039/DT9890001925.

28. Peisach, J., and Blumberg, W.E. (1974). Structural implications derived from the analysis of electron paramagnetic resonance spectra of natural and artificial copper

proteins. Arch. Biochem. Biophys. *165*, 691–708. https://doi.org/10.1016/0003-9861(74)90298-7.

29. Zha, R.H., Delparastan, P., Fink, T.D., Bauer, J., Scheibel, T., and Messersmith, P.B. (2019). Universal nanothin silk coatings via controlled spidroin self-assembly. Biomater. Sci. *7*, 683–695. https://doi.org/10.1039/C8BM01186A.

30. Cao, Y., and Li, H. (2007). Polyprotein of GB1 is an ideal artificial elastomeric protein. Nat. Mater. *6*, 109–114. https://doi.org/10.1038/nmat1825.

31. Puchner, E.M., and Gaub, H.E. (2009). Force and function: probing proteins with AFM-based force spectroscopy. Curr. Opin. Struct. Biol. *19*, 605–614. https://doi.org/10.1016/j.sbi.2009.09.005.

32. Delparastan, P., Malollari, K.G., Lee, H., and Messersmith, P.B. (2019). Direct evidence for the polymeric nature of polydopamine. Angew. Chem. Int. Ed. *58*, 1077–1082. https://doi.org/10.1002/anie.201811763.

33. Malollari, K.G., Delparastan, P., Sobek, C., Vachhani, S.J., Fink, T.D., Zha, R.H., and Messersmith, P.B. (2019). Mechanical enhancement of bioinspired polydopamine nanocoatings. ACS Appl. Mater. Inter. *11*, 43599–43607. https://doi.org/10.1021/acsami.9b15740.

34. Huang, Z., Delparastan, P., Burch, P., Cheng, J., Cao, Y., and Messersmith, P.B. (2018). Injectable dynamic covalent hydrogels of boronic acid polymers cross-linked by bioactive plant-derived polyphenols. Biomater. Sci. *6*, 2487–2495. https://doi.org/10.1039/C8BM00453F.

35. Li, Y., Wen, J., Qin, M., Cao, Y., Ma, H., and Wang, W. (2017). Single-molecule mechanics of catechol-iron coordination bonds. ACS Biomater. Sci. Eng. *3*, 979–989. https://doi.org/10.1021/acsbiomaterials.7b00186.

36. Hosono, N., Kushner, A.M., Chung, J., Palmans, A.R.A., Guan, Z., and Meijer, E.W. (2015). Forced unfolding of single-chain polymeric nanoparticles. J. Am. Chem. Soc. *137*, 6880–6888. https://doi.org/10.1021/jacs.5b02967.

37. Liu, R., Deng, Q., Yang, Z., Yang, D., Han, M.-Y., and Liu, X.Y. (2016). "Nano-fishnet" structure making silk fibers tougher. Adv. Funct. Mater. *26*, 5534–5541. https://doi.org/10.1002/adfm.201600813.

38. Oberhauser, A.F., Marszalek, P.E., Carrion-Vazquez, M., and Fernandez, J.M. (1999). Single protein misfolding events captured by atomic force microscopy. Nat. Struct. Biol. *6*, 1025–1028. https://doi.org/10.1038/14907.

39. Xue, Y., Li, X., Li, H., and Zhang, W. (2014). Quantifying thiol–gold interactions towards the efficient strength control. Nat. Commun. *5*, 4348. https://doi.org/10.1038/ncomms5348.

40. Zheng, P., Chou, C.-C., Guo, Y., Wang, Y., and Li, H. (2013). Single molecule force spectroscopy reveals the molecular mechanical anisotropy of the FeS 4 metal center in rubredoxin. J. Am. Chem. Soc. *135*, 17783–17792. https://doi.org/10.1021/ja406695g.

41. Sun, W., Xue, B., Fan, Q., Tao, R., Wang, C., Wang, X., Li, Y., Qin, M., Wang, W., Chen, B., et al. (2020). Molecular engineering of metal coordination interactions for strong, tough, and fast-recovery hydrogels. Sci. Adv. *6*, eaaz9531. https://doi.org/10.1126/sciadv.aaz9531.

42. Oroudjev, E., Soares, J., Arcidiacono, S., Thompson, J.B., Fossey, S.A., and Hansma, H.G. (2002). Segmented nanofibers of spider dragline silk: atomic force microscopy and single-molecule force spectroscopy. Proc. Natl. Acad. Sci. *99*, 6460–6465. https://doi.org/10.1073/pnas.082526499.

43. Stirnemann, G., Giganti, D., Fernandez, J.M., and Berne, B.J. (2013). Elasticity, structure, and relaxation of extended proteins under force. Proc. Natl. Acad. Sci. *110*, 3847–3852. https://doi.org/10.1073/pnas.1300596110.

44. Schilling, K.M., Tao, L., Wu, B., Kiblen, J.T.M., Ubilla-Rodriguez, N.C., Pushie, M.J., Britt, R.D., Roseman, G.P., Harris, D.A., and Millhauser, G.L. (2020). Both N-terminal and C-terminal histidine residues of the prion protein are essential for copper coordination and neuroprotective self-regulation. J. Mol. Biol. *432*, 4408–4425. https://doi.org/10.1016/j.jmb.2020.05.020.

45. Millhauser, G.L. (2007). Copper and the prion protein: methods, structures, function, and disease. Annu. Rev. Phys. Chem. *58*, 299–320. https://doi.org/10.1146/annurev.physchem.58.032806.104657.

46. Chattopadhyay, M., Walter, E.D., Newell, D.J., Jackson, P.J., Aronoff-Spencer, E., Peisach, J., Gerfen, G.J., Bennett, B., Antholine, W.E., and Millhauser, G.L. (2005). The octarepeat domain of the prion protein binds Cu(II) with three distinct coordination modes at pH 7.4. J. Am. Chem. Soc. *127*, 12647–12656. https://doi.org/10.1021/ja053254z.

47. Solomon, E.I., Sundaram, U.M., and Machonkin, T.E. (1996). Multicopper oxidases and oxygenases. Chem. Rev. *96*, 2563–2606. https://doi.org/10.1021/cr950046o.

48. Kang, M., Myung, S.J., and Jin, H.-J. (2006). Nylon 610 and carbon nanotube composite by in situ interfacial polymerization. Polymer (Guildf) *47*, 3961–3966. https://doi.org/10.1016/j.polymer.2006.03.073.

49. Harrington, M.J., and Waite, J.H. (2008). pH-dependent locking of giant mesogens in fibers drawn from mussel byssal collagens. Biomacromolecules *9*, 1480–1486. https://doi.org/10.1021/bm8000827.

50. Fu, J., Guerette, P.A., Pavesi, A., Horbelt, N., Lim, C.T., Harrington, M.J., and Miserez, A. (2017). Artificial hagfish protein fibers with ultra-high and tunable stiffness. Nanoscale *9*, 12908–12915. https://doi.org/10.1039/c7nr02527k.

51. Bell, E., and Gosline, J. (1996). Mechanical design of mussel byssus: material yield enhances attachment strength. J. Exp. Biol. *199*, 1005–1017. https://doi.org/10.1242/jeb.199.4.1005.

52. Gosline, J., Lillie, M., Carrington, E., Guerette, P., Ortlepp, C., and Savage, K. (2002). Elastic proteins: biological roles and mechanical properties. Philos. Trans. R. Soc. Lond. Ser. B

Biol. Sci. *357*, 121–132. https://doi.org/10.1098/rstb.2001.1022.

53. Gosline, J.M., Guerette, P.A., Ortlepp, C.S., and Savage, K.N. (1999). The mechanical design of spider silks: from fibroin sequence to mechanical function. J. Exp. Biol. *202*, 3295–3303. https://doi.org/10.1242/jeb.202.23.3295.

54. Filippidi, E., Cristiani, T.R., Eisenbach, C.D., Waite, J.H., Israelachvili, J.N., Ahn, B.K., and Valentine, M.T. (2017). Toughening elastomers using mussel-inspired iron-catechol complexes. Science *358*, 502–505. https://doi.org/10.1126/science.aao0350.

55. Wang, J., Cohen Stuart, M.A., and van der Gucht, J. (2012). Phase diagram of coacervate complexes containing reversible coordination structures. Macromolecules *45*, 8903–8909. https://doi.org/10.1021/ma301690t.

56. Singh, V., Xu, L., Boyko, S., Surewicz, K., and Surewicz, W.K. (2020). Zinc promotes liquid–liquid phase separation of tau protein. J. Biol. Chem. *295*, 5850–5856. https://doi.org/10.1074/jbc.AC120.013166.

57. Ray, S., Singh, N., Kumar, R., Patel, K., Pandey, S., Datta, D., Mahato, J., Panigrahi, R., Navalkar, A., Mehra, S., et al. (2020). α-Synuclein aggregation nucleates through liquid–liquid phase separation. Nat. Chem. *12*, 705–716. https://doi.org/10.1038/s41557-020-0465-9.

58. Uversky, V.N., Kuznetsova, I.M., Turoverov, K.K., and Zaslavsky, B. (2015). Intrinsically disordered proteins as crucial constituents of cellular aqueous two phase systems and coacervates. FEBS Lett. *589*, 15–22. https://doi.org/10.1016/j.febslet.2014.11.028.

59. Martin, E.W., and Mittag, T. (2018). Relationship of sequence and phase separation in protein low-complexity regions. Biochemistry *57*, 2478–2487. https://doi.org/10.1021/acs.biochem.8b00008.

60. Hwang, D.S., Zeng, H., Srivastava, A., Krogstad, D.V., Tirrell, M., Israelachvili, J.N., and Waite, J.H. (2010). Viscosity and interfacial properties in a mussel-inspired adhesive coacervate. Soft Matter *6*, 3232. https://doi.org/10.1039/c002632h.

61. Brutchey, R.L., and Morse, D.E. (2008). Silicatein and the translation of its molecular mechanism of biosilicification into low temperature nanomaterial synthesis. Chem. Rev. *108*, 4915–4934. https://doi.org/10.1021/cr078256b.

62. Miserez, A., Rubin, D., and Waite, J.H. (2010). Cross-linking chemistry of squid beak. J. Biol. Chem. *285*, 38115–38124. https://doi.org/10.1074/jbc.M110.161174.

63. Wang, S.X., Mure, M., Medzihradszky, K.F., Burlingame, A.L., Brown, D.E., Dooley, D.M., Smith, A.J., Kagan, H.M., and Klinman, J.P. (1996). A crosslinked cofactor in lysyl oxidase: redox function for amino acid side chains. Science *273*, 1078–1084. https://doi.org/10.1126/science.273.5278.1078.

64. Kaim, W., and Rall, J. (1996). Copper—a"Modern" bioelement. Angew. Chem. Int. Ed. English *35*, 43–60. https://doi.org/10.1002/anie.199600431.

65. Brown, K.C., Yang, S.-H., and Kodadek, T. (1995). Highly specific oxidative crosslinking of proteins mediated by a nickel-peptide

complex. Biochemistry *34*, 4733–4739. https://doi.org/10.1021/bi00014a030.

66. Afgan, E., Baker, D., van den Beek, M., Blankenberg, D., Bouvier, D., Čech, M., Chilton, J., Clements, D., Coraor, N., Eberhard, C., et al. (2016). The Galaxy platform for accessible, reproducible and collaborative biomedical analyses: 2016 update. Nucleic Acids Res. *44*, W3–W10. https://doi.org/10.1093/nar/gkw343.

67. Haas, B.J., Papanicolaou, A., Yassour, M., Grabherr, M., Blood, P.D., Bowden, J., Couger, M.B., Eccles, D., Li, B., Lieber, M., et al. (2013). De novo transcript sequence reconstruction from RNA-seq using the Trinity platform for reference generation and analysis. Nat. Protoc. *8*, 1494–1512. https://doi.org/10.1038/nprot.2013.084.

68. Li, B., and Dewey, C.N. (2011). RSEM: accurate transcript quantification from RNA-Seq data with or without a reference genome. BMC Bioinformatics *12*, 323. https://doi.org/10.1186/1471-2105-12-323.

69. Winder, A.J., and Harris, H. (1991). New assays for the tyrosine hydroxylase and dopa oxidase activities of tyrosinase. Eur. J. Biochem. *198*, 317–326. https://doi.org/10.1111/j.1432-1033.1991.tb16018.x.

70. Rodriguezlopez, J.N., Escribano, J., and Garciacanovas, F. (1994). A continuous spectrophotometric method for the determination of monophenolase activity of tyrosinase using 3-Methyl-2-benzothiazolinone hydrazone. Anal. Biochem. *216*, 205–212. https://doi.org/10.1006/abio.1994.1026.

71. Napolitano, A., Pezzella, A., Vincensi, M.R., and Prota, G. (1995). Oxidative degradation of melanins to pyrrole acids: a model study. Tetrahedron *51*, 5913–5920. https://doi.org/10.1016/0040-4020(95)00259-B.

72. Ito, S. (1986). Reexamination of the structure of eumelanin. Biochim. Biophys. Acta - Gen. Subj. *883*, 155–161. https://doi.org/10.1016/0304-4165(86)90146-7.

73. Ito, S., Wakamatsu, K., and Ozeki, H. (1993). Spectrophotometric assay of eumelanin in tissue samples. Anal. Biochem. *215*, 273–277. https://doi.org/10.1006/abio.1993.1586.

74. Vandebril, S., Franck, A., Fuller, G.G., Moldenaers, P., and Vermant, J. (2010). A double wall-ring geometry for interfacial shear rheometry. Rheol. Acta *49*, 131–144. https://doi.org/10.1007/s00397-009-0407-3.

Supplemental information

A multi-tasking polypeptide

from bloodworm jaws: Catalyst, template,

and copolymer in film formation

William R. Wonderly, Tuan T.D. Nguyen, Katerina G. Malollari, Daniel DeMartini, Peyman Delparastan, Eric Valois, Phillip B. Messersmith, Matthew E. Helgeson, and J. Herbert Waite

**SUPPLEMENTAL EXPERIMENTAL PROCEDURES**

AFM-assisted Force Spectroscopy:

Single molecule force spectroscopy (SMFS) experiments were performed using a JPK ForceRobot300 Atomic Force Microscope (JPK Instruments AG, Berlin, Germany). For SMFS experiments, soft silicon nitride cantilevers (MLCT from Bruker Nano Inc., USA) of typical spring constant of 50-60 pN/nm were used. The experiments were performed after allowing the cantilever to equilibrate in solution and calibrating the sensitivity and spring constant of all the cantilevers using the equipartition theorem.[1] Silicon wafers with a 100 nm titanium oxide (TiO_2) layer (University Wafer, Inc, Boston, MA) were used as substrate for our experiments. TiO_2 substrates were first cleaned with a 3:1 mixture of water and Simple Green solution for degreasing by placing into sonication bath for 15 minutes. The substrates were then rinsed and sonicated with water followed by isopropanol and acetone, each for 15 minutes, and dried under a stream of nitrogen. SMFS samples were prepared by drop casting an aqueous mixture solution of MTP and Cu^{2+} (as $CuSO_4$) at final concentrations of 4.5 µM and 36 µM, respectively, in 100 mM MOPS buffer at pH 7.4 on TiO_2 substrates. Based on the concentrations of the mixture and MTP composition, we estimate a relative ratio of Cu^{2+}:MTP of 8:1 or alternatively Cu^{2+}:His 1:10 in the final solution. After evaporation of solvent, the MTP-Cu^{2+} film coated TiO_2 substrates were briefly rinsed with 1ml buffer and placed in AFM sample holder which was later filled with 100 mM MOPS buffer at pH 7.4. In a typical SMFS measurement, the cantilever was approached to the surface with a piezo velocity of 500 nm/s, a contact force of ~2nN, and a dwelling time (contact time between probe and surface) of 1s over a z-piezo range of 600 nm. During the SMFS experiments more than thousands of force-extension (F-X) curves were collected on multiple samples (n=3-5) to achieve statistically representative datasets. Data obtained in the SMFS experiments were analyzed using the JPK data processing software and a home-written procedure in IgorPro (Wavemetrics) for fitting the stretching events in the F-X curves with the Worm-like Chain (WLC) model to measure the corresponding rupture force and contour length. Histograms of the rupture forces and contour lengths were plotted using the OriginPro software. No previous studies have been performed to report the persistence length for MTP; however, previous reports have shown values of 0.38 nm or less for PEG,[2] 0.38 nm for amyloid fibers,[3] and 0.4 nm for polyproteins and polypeptides.[4,5] WLC fitting of the rupture events for MTP-Cu^{2+} complexes yielded a persistence length of ~0.4 nm which is consistent with the values reported for stretching a flexible single protein macromolecule in aqueous solution.

$$F = \frac{kT}{p} * \left(\frac{1}{4\left(1 - \frac{x}{L_c}\right)^2} - \frac{1}{4} + \frac{x}{L_c} \right)$$

The WLC model[6] used for fitting where F is the applied force, p is the persistence length, k is the Boltzmann constant, L_c is the contour length, and T is the absolute temperature, has previously been used to analyze the behavior of macromolecules in adsorbed films such as the ones in this study.[7–9]

From the tens of thousands of F-X curves collected, ~2.2% (typical range for single molecule studies) contained the signature sawtooth pattern. The rest of the data either did not show similar stretching events or contained only individual non-specific rupture events (i.e. protein-substrate/cantilever interactions). Here were only selected F-X curves with sawtooth pattern of three or more dissociation events for data analysis to further separate the non-specific interactions from the specific interactions corresponding to the rupture of copper-ligand bonds. Moreover, we performed a number of control experiments on Cu^{2+}-free MTP or EDTA-MTP-Cu^{2+} films to further confirm the nature of sawtooth dissociation peaks. The sawtooth pattern was not observed in either of the control experiments. In the case of Cu^{2+}-free MTP films, F-X curves were completely distinct from the sawtooth-like events and generally consisted of single peaks at short distances and high rupture forces (>500 pN) corresponding to the detachment of protein chain from either the surface of the substrate or the cantilever. Next, we performed SMFS on Cu^{2+}-MTP in the presence of 90 mM Cu-chelating agent EDTA. In the presence of such a high ratio of EDTA:Cu^{2+} (2500:1), we expect that Cu^{2+} is essentially bound to the chelating agent and is not available for interacting with less thermodynamically favorable residues in MTP sequence. As a result, the MTP-Cu^{2+} interactions could not be established in the presence of EDTA and therefore we did not observe sawtooth pattern in the F-X curves that were previously detected for MTP-Cu^{2+} in the absence of chelating agents.
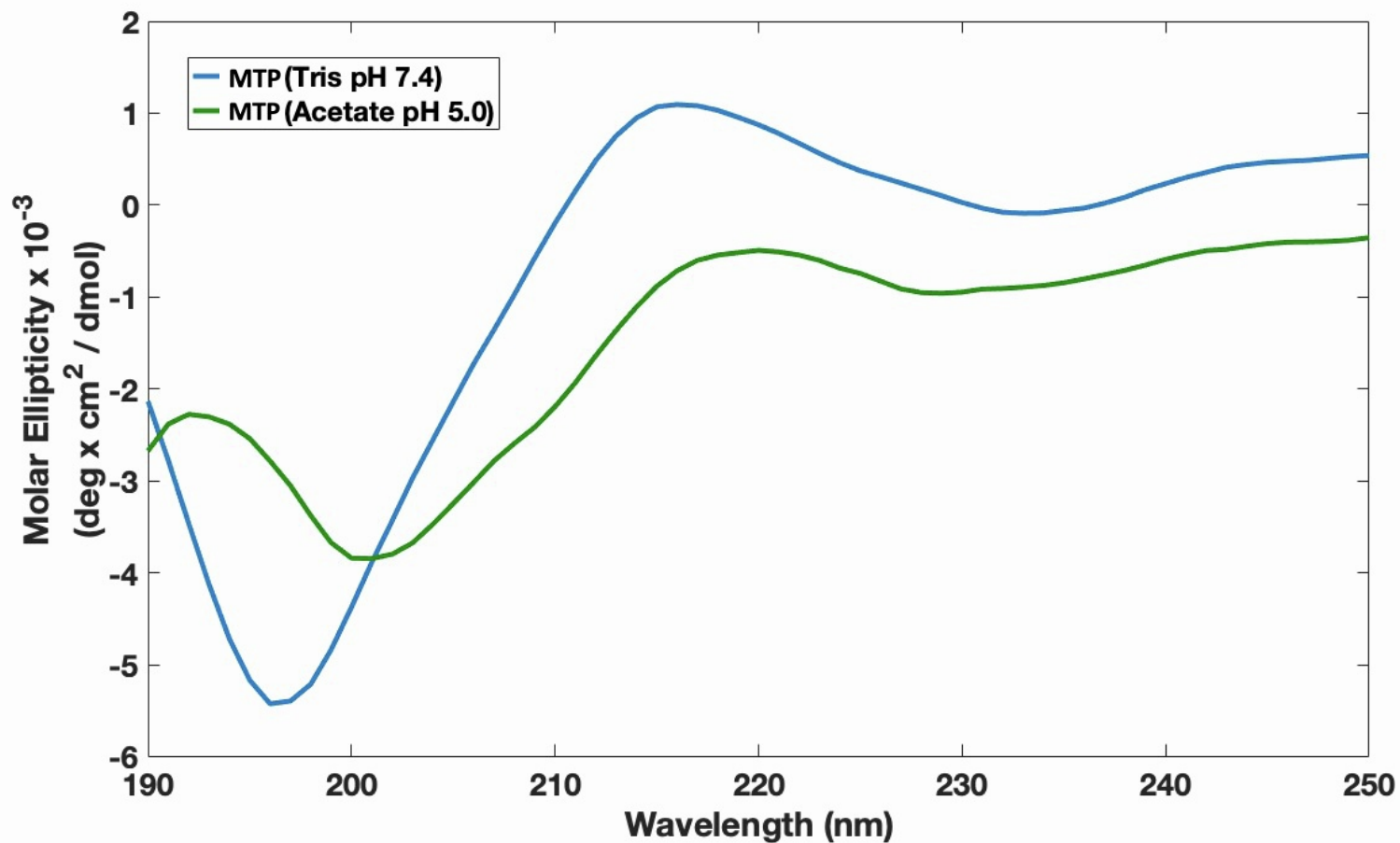
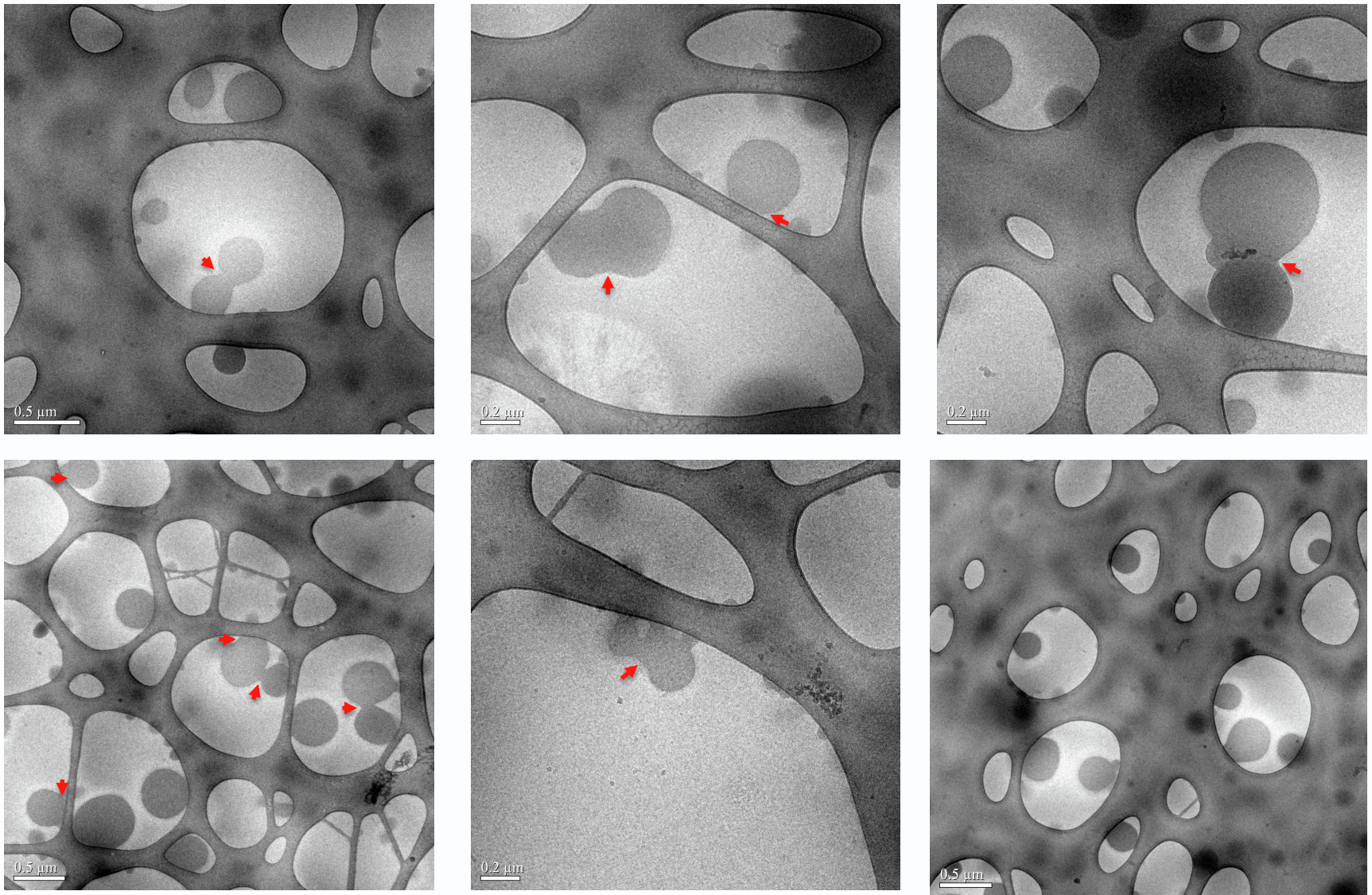**Figure S1. Solution conformation of MTP as a function of pH**. The blue curve is 50µM MTP in 100mM Tris (pH 7.4). The green curve is 50µM MTP in 100mM sodium acetate buffer (pH 5).
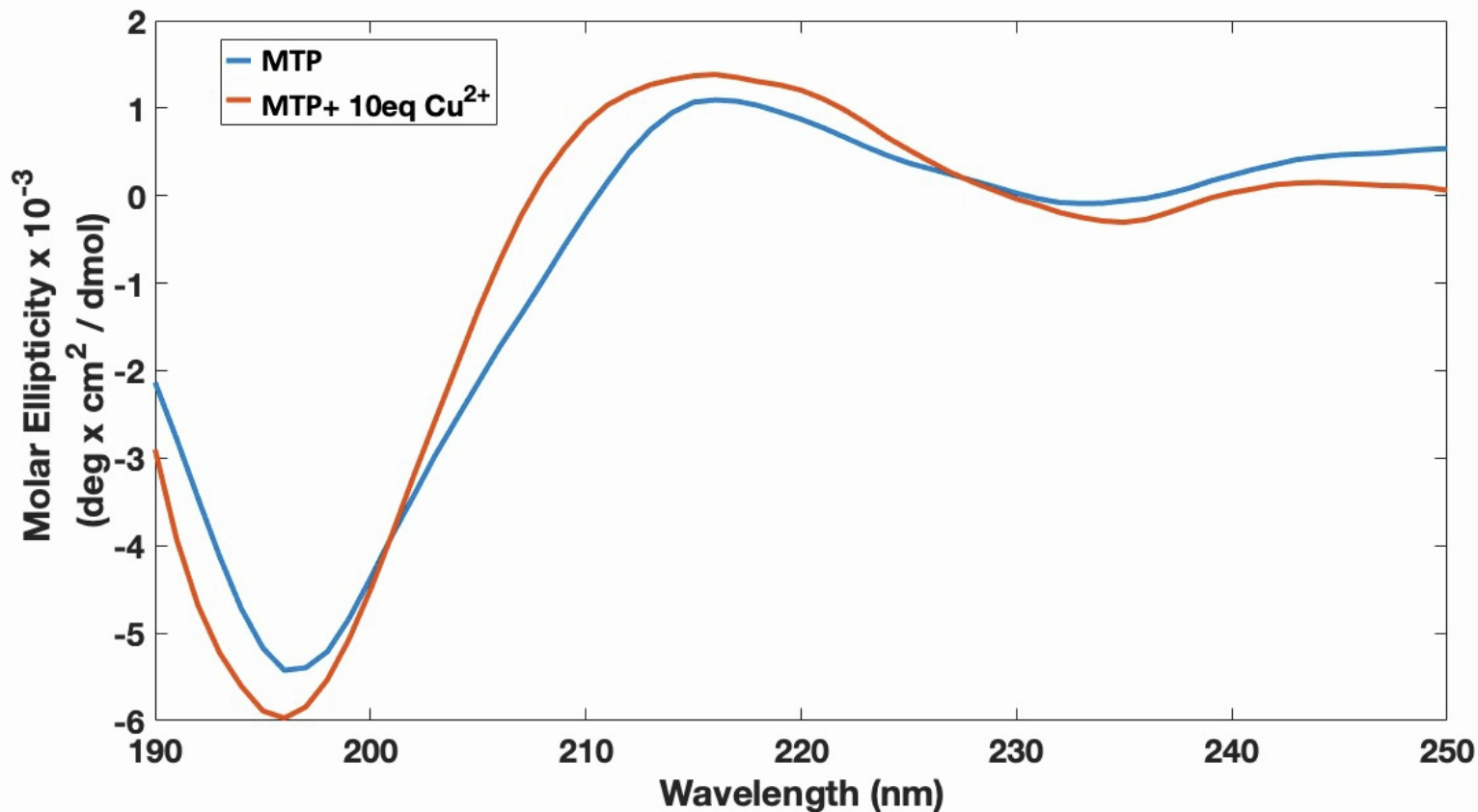
**Figure S2. Copper dependence of MTP solution conformation**. The blue curve is of 50µM MTP in 50 mM Tris (pH 7.4). The red curve is of 50µM MTP in Tris (pH 7.4) supplemented with 100µM $CuSO_4$.

**Figure S3. Additional Cryo-TEM Images of MTP droplet wetting and fusion.** Supplemental Cryo TEM of 5 μM MTP with 50 μM $CuSO_4$ included in 50mM Tris buffer (pH = 7.5). Red arrows indicate locations of droplet fusion or wetting of the lacey carbon support.
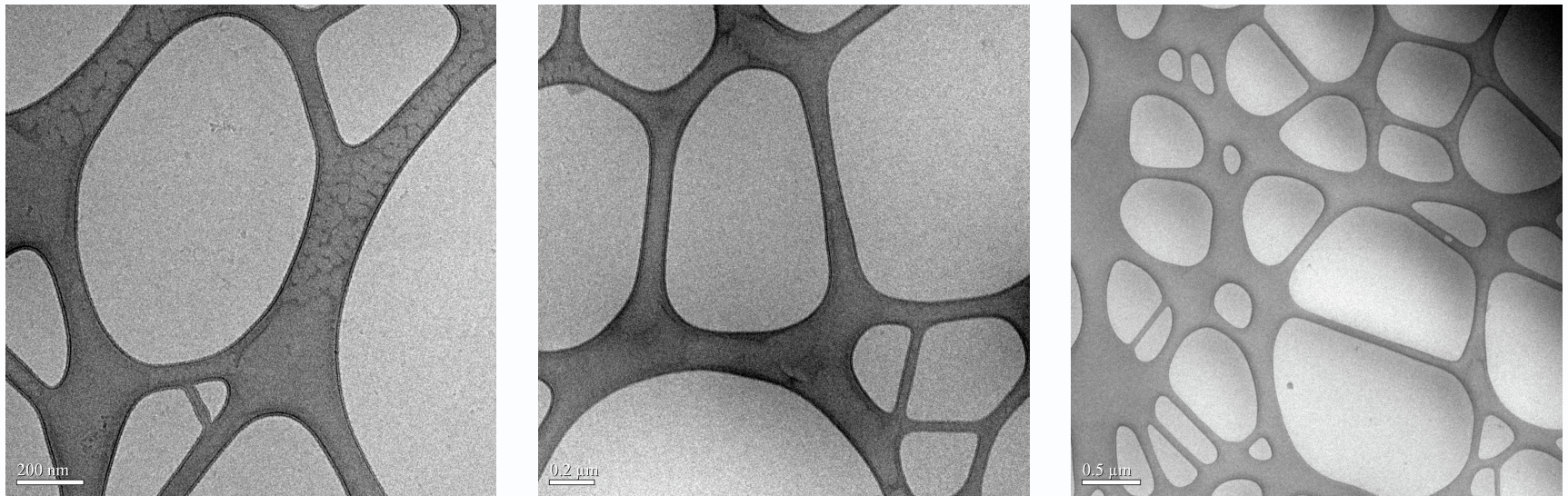
Figure S4. Cryo-TEM In the absence of Cu^{2+}. The Cryo TEM of 5 μM MTP in 50mM Tris buffer (pH = 7.5) shows no evidence of phase separation.
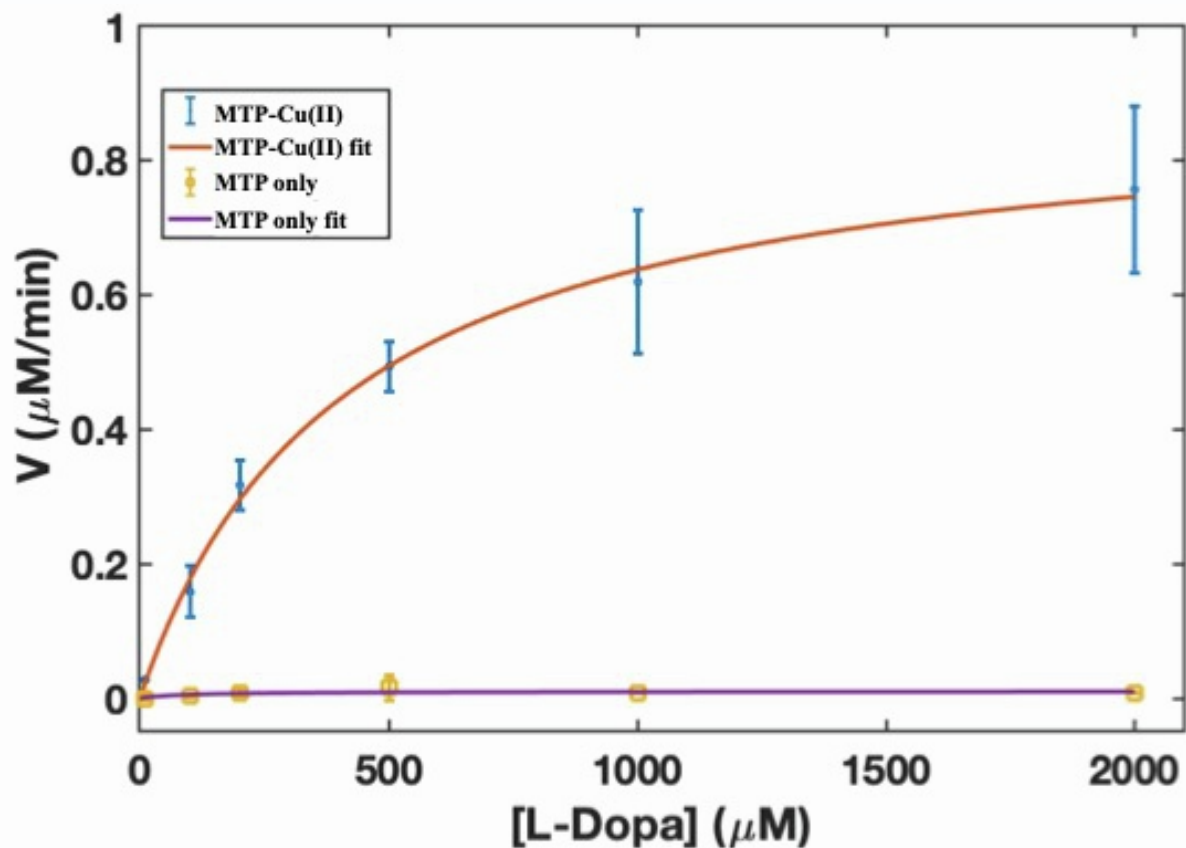
Figure S5. Catalytic properties of Copper-bound MTP. Reaction rate dependence of L-Dopa oxidation to form the MBTH-quinone adduct carried out in Tris buffer (50mM) pH 7.4 in the presence of 5μM MTP loaded with 10 eq. $CuSO_4$ (black circles). The blue circles represent the experimentally determined reaction rates of MS-Cu^{2+} with L-Dopa, the solid red line represents a fit of the data to the Michaelis-Menten equation. The yellow squares are the copper-free MTP reaction rates, and the solid purple line its Michaelis-Menten fit.
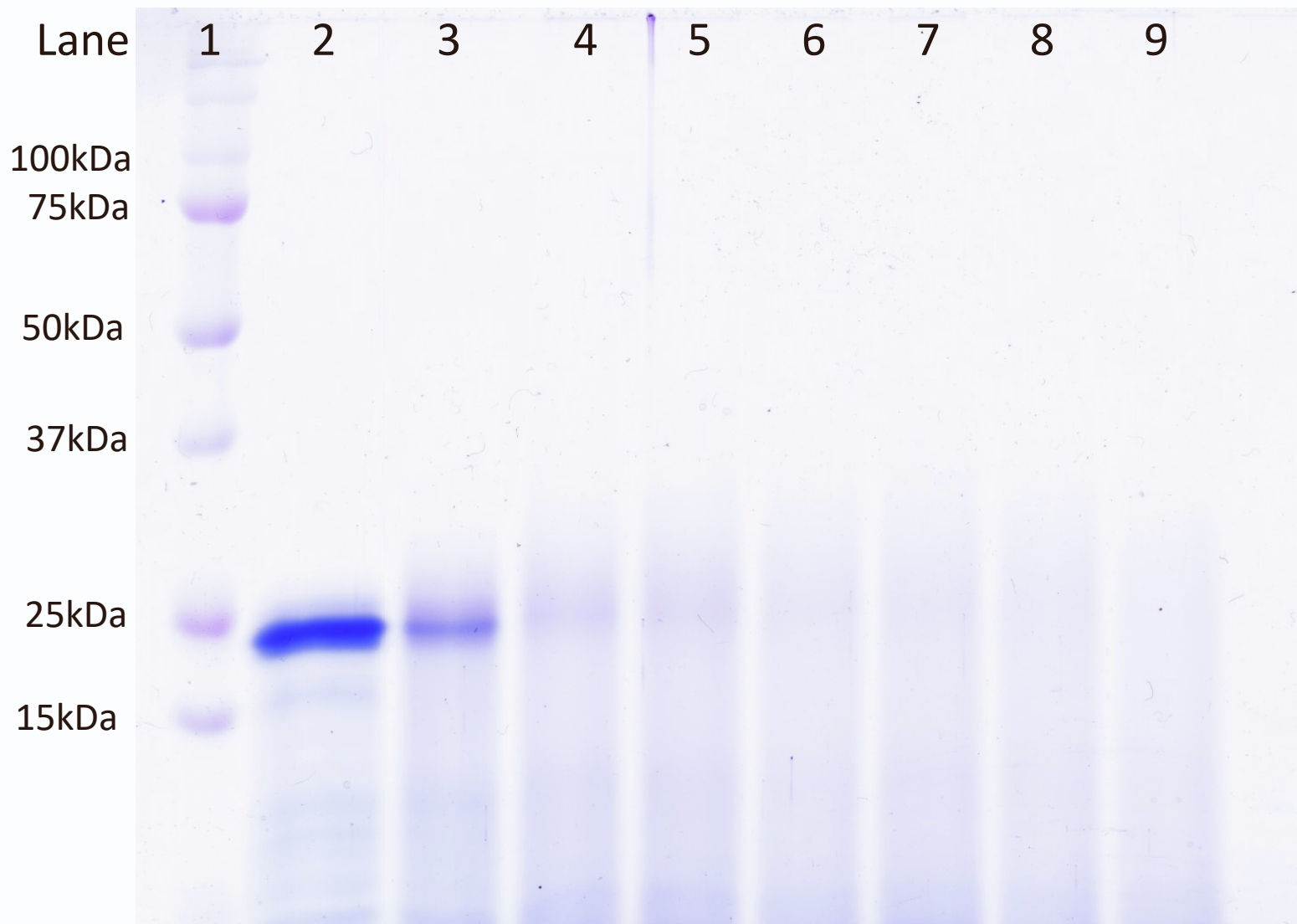
Figure S6. Time course of MTP-melanin reaction as monitored by SDS-PAGE. The reaction contained 5μM MTP, 50μM $CuSO_4$, 100mM Tris (pH 7.4) and 0.5mM L-Dopa. The first lane is the ladder and lanes 2-9 represent t=0, 15min, 30min, 45 min, 1hr, 2hr, 4hr, and 12hr.
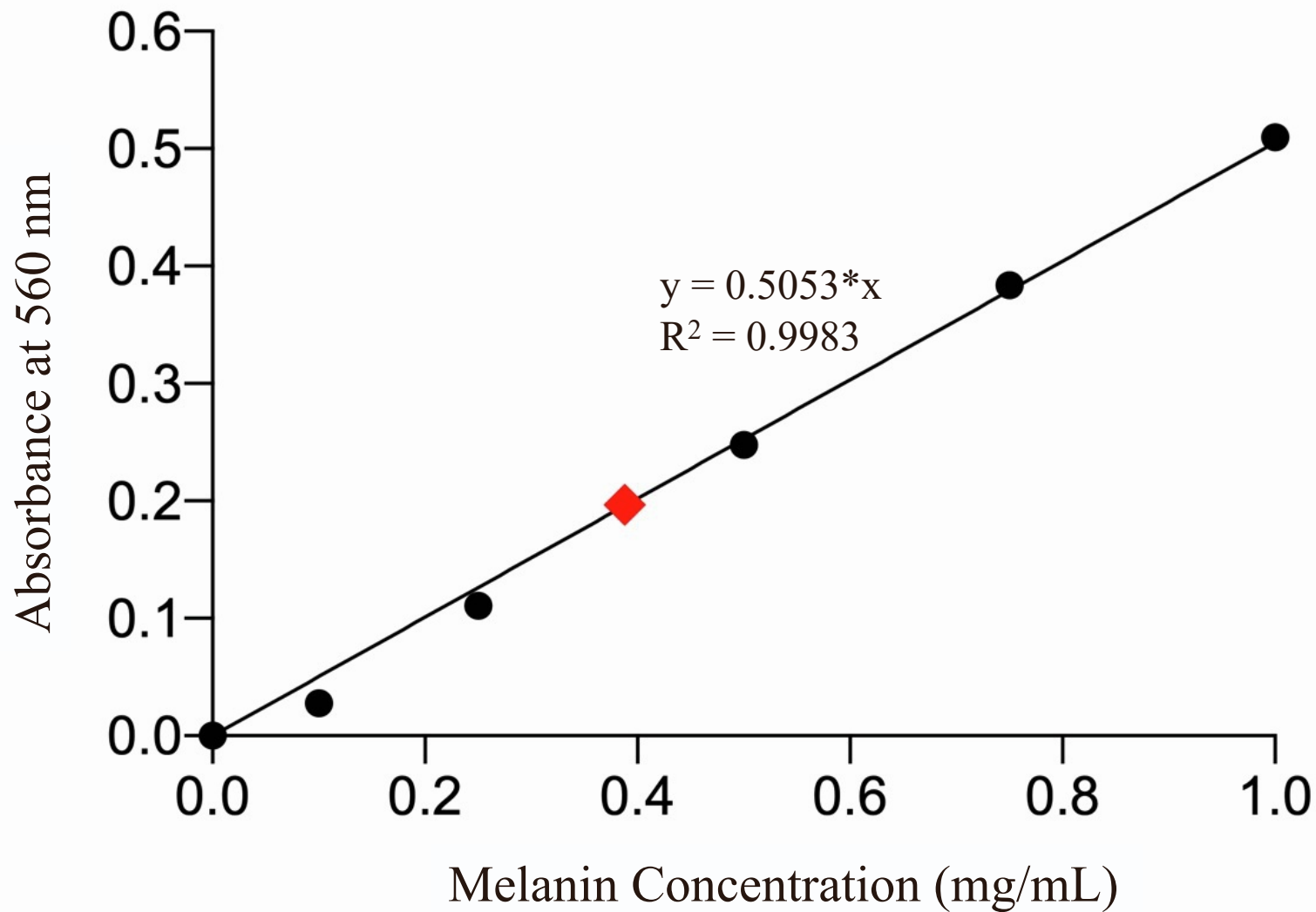
Figure S7. Determination of Melanin degradation products. A standard curve was created by dissolving synthetic melanin in alkaline peroxide at 0.1, 0.2, 0.5, 0.75, and 1 mg/mL (black dots) and measuring the absorbance of the degradation products at 560nm. A sample of washed and isolated MTP-melanin films was similarly prepared at 4 mg/mL and its absorbance measured to be 0.197 AU which corresponds to a melanin concentration of 0.4 mg/mL, or 10% melanin by mass. The best fit line was forced to have an Y-intercept of 0.
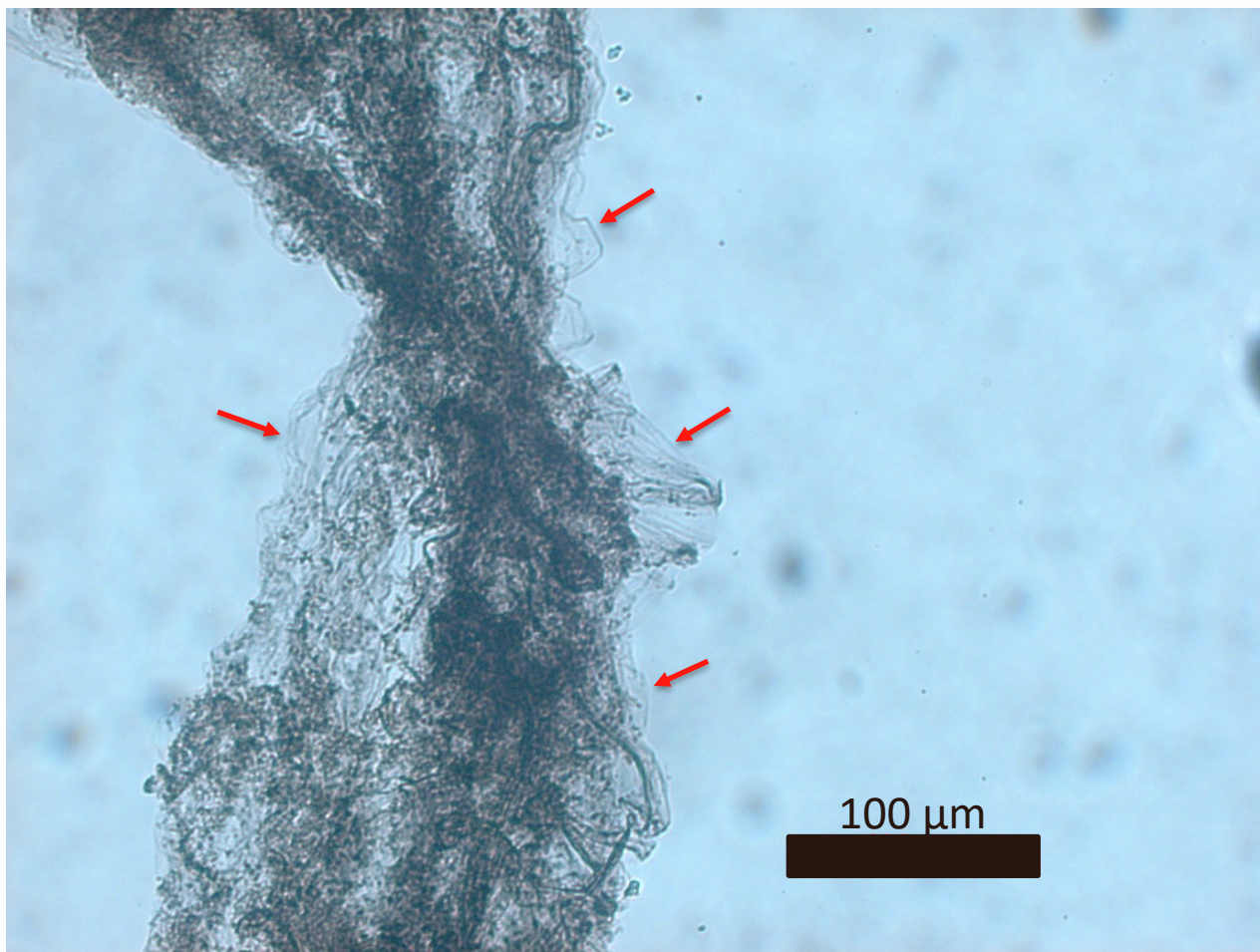
Figure S8. Microscopic observation of MTP-melanin films. When observed under a microscope, interfacial films appear black indicating melanization. We also observe what appear to be folds (red arrows) around the edges of the collected film where only one layer is present.
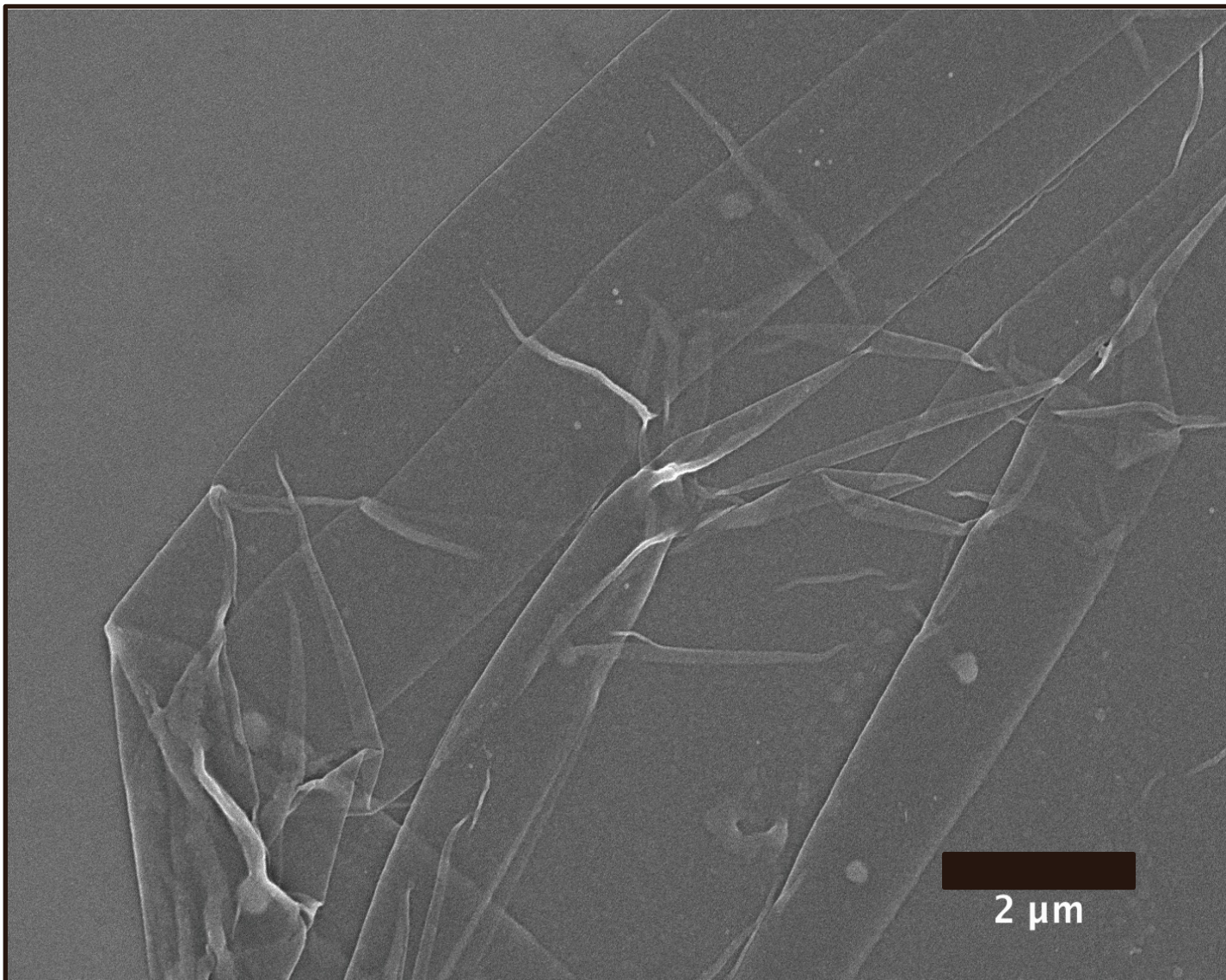
Figure S9. SEM image of an MTP catalyzed melanin film. MTP-melanin films were allowed to react for 30 minutes and transferred to a silicon substrate.

1. Lübbe, J., Temmen, M., Rahe, P., Kühnle, A., and Reichling, M. (2013). Determining cantilever stiffness from thermal noise. Beilstein J. Nanotechnol. *4*, 227–233. 10.3762/bjnano.4.23.
2. Kienberger, F., Pastushenko, V.P., Kada, G., Gruber, H.J., Riener, C., Schindler, H., and Hinterdorfer, P. (2000). Static and Dynamical Properties of Single Poly(Ethylene Glycol) Molecules Investigated by Force Spectroscopy. Single Mol. *1*, 123–128. 10.1002/1438-5171(200006)1:2<123::AID-SIMO123>3.0.CO;2-3.
3. Kellermayer, M.S.Z., Grama, L., Karsai, Á., Nagy, A., Kahn, A., Datki, Z.L., and Penke, B. (2005). Reversible Mechanical Unzipping of Amyloid β-Fibrils. J. Biol. Chem. *280*, 8464–8470. 10.1074/jbc.M411556200.
4. Ott, W., Jobst, M.A., Bauer, M.S., Durner, E., Milles, L.F., Nash, M.A., and Gaub, H.E. (2017). Elastin-like Polypeptide Linkers for Single-Molecule Force Spectroscopy. ACS Nano *11*, 6346–6354. 10.1021/acsnano.7b02694.
5. Li, Y., Cheng, J., Delparastan, P., Wang, H., Sigg, S.J., DeFrates, K.G., Cao, Y., and Messersmith, P.B. (2020). Molecular design principles of Lysine-DOPA wet adhesion. Nat. Commun. *11*, 1–8. 10.1038/s41467-020-17597-4.
6. Bustamante, C., Marko, J.F., Siggia, E.D., and Smith, S. (1994). Entropic Elasticity of λ-Phage DNA. Science (80-.). *265*, 1599–1600. 10.1126/science.8079175.
7. Zha, R.H., Delparastan, P., Fink, T.D., Bauer, J., Scheibel, T., and Messersmith, P.B. (2019). Universal nanothin silk coatings: Via controlled spidroin self-assembly. Biomater. Sci. *7*, 683–695.
8. Bemis, J.E., Akhremitchev, B.B., and Walker, G.C. (1999). Single Polymer Chain Elongation by Atomic Force Microscopy. Langmuir *15*, 2799–2805. 10.1021/la980853t.
9. Delparastan, P., Malollari, K.G., Lee, H., and Messersmith, P.B. (2019). Direct Evidence for the Polymeric Nature of Polydopamine. Angew. Chemie Int. Ed. *58*, 1077–1082. 10.1002/anie.201811763.